Direct measurement of surface forces: Recent advances and insights

Direct measurement of surface forces: recent advances and insights

Weifeng Lin and Jacob Klein[a)]

Affiliations

Department of Molecular Chemistry and Materials Science, Weizmann Institute of Science, 76100 Rehovot, Israel

a) Author to whom correspondence should be addressed: jacob.klein@weizmann.ac.il

PLEASE CITE THIS ARTICLE AS DOI: 10.1063/5.0059893

Abstract

The direct measurement of forces between atomically-smooth mica surfaces down to sub-nanometer separations was pioneered over 50 years ago, and has yielded deep understanding of a range of interfacial effects, not least the forces that determine colloidal stability and self-assembly, the properties of highly confined fluids and the molecular origins of friction and lubrication. Here we describe recent advances, including the use of substrates other than mica; probing the shear properties of highly-confined fluids including hydration layers; and the modulation of surface forces by surface-attached macromolecules and amphiphiles, together with microscopic imaging of surface morphology. These advances enabled novel features such as external potential control of the interacting surfaces, new understanding of lubrication in aqueous and biological systems, the design of novel nanoparticles and surface assemblies for modulating frictional dissipation, and insight into the nature of long-ranged attraction between surfactant-hydrophobized surfaces. We conclude by briefly outlining future challenges and opportunities provided by such direct surface force studies.

Table of contents

I. Introduction

The direct measurement of both normal and shear forces between two smooth macroscopic surfaces as a function of their absolute separation D, with Å-level resolution in D, enables a large range of interfacial properties to be examined, not least the forces that determine colloidal and macromolecular interactions, as well as frictional dissipation at the molecular level. Tabor and his students Winterton and Israelachvili, starting in the late 1960s, pioneered such measurements for direct determination of van der Waals forces acting between two molecularly smooth mica surfaces in air,[1,2] where the high resolution in D was provided by white-light multiple beam interferometry. Subsequently Israelachvili and coworkers extended this approach to measure surface forces across

liquids and solutions[3-5] (calling their measurement system a surface force apparatus, SFA) and shortly after that Klein extended it to measure interactions between surface-attached polymers,[6,7] using a different device he called a surface force balance (SFB). The original SFA and SFB were later extended to different configurations, and to measurements of a wide variety of different interactions including structural forces,[5,8] hydrophobic interactions,[9,10] DLVO interactions (van der Waals and electrostatic double layer),[11,12] hydration forces,[13-15] and other more specific forces[16-18] related to polymer or living systems. To avoid confusion, we shall henceforth refer to all different configurations of the apparatus used to measure surface forces directly between macroscopic, smooth surfaces as SFBs, since they all essentially act by *balancing* the surface forces against the bending of mechanical springs in the apparatus (see figure 1), and thereby obtaining their magnitude. Shear force measurements using this approach were also pioneered by Tabor and Israelachvili,[19] to explore the frictional properties of calcium stearate monolayers and multilayers deposited between mica surfaces, and this was extended by Israelachvili and coworkers for measuring frictional forces in the SFB.[20-25] Klein and coworkers[16,26] designed a new device which could probe shear forces with significantly improved sensitivity and resolution with respect to the previous designs, enabling the very low frictional coefficients between polymeric layers to be measured. To illustrate the general principle, a schematic of the SFB as developed by the Klein group[16,26,27] is shown in figure 1. The separation D between the surfaces may be measured (down to 1-2 Å resolution) by monitoring the wavelengths of fringes of equal chromatic order (FECO) arising through multiple beam interferometry. Visualizing the fringes also allows for directly measuring the true contact area between the surfaces (and thereby the mean pressure between them), and following any surface deformations occurring in the contact region. The shear forces $F_s(D)$ (with a resolution of ca. 100

nN, limited by ambient noise) and normal forces $F_n(D)$ (with a resolution of ca. 10 nN) between the surfaces are measured via Hooke's law by monitoring the bending of two vertical leaf springs S_1 and a horizontal leaf spring S_2. The bending of the vertical leaf springs (ΔD) is measured by using an air-gap capacitor. The bending of the horizontal leaf-spring (ΔX) is determined by monitoring the changes in the wavelength of the FECO.

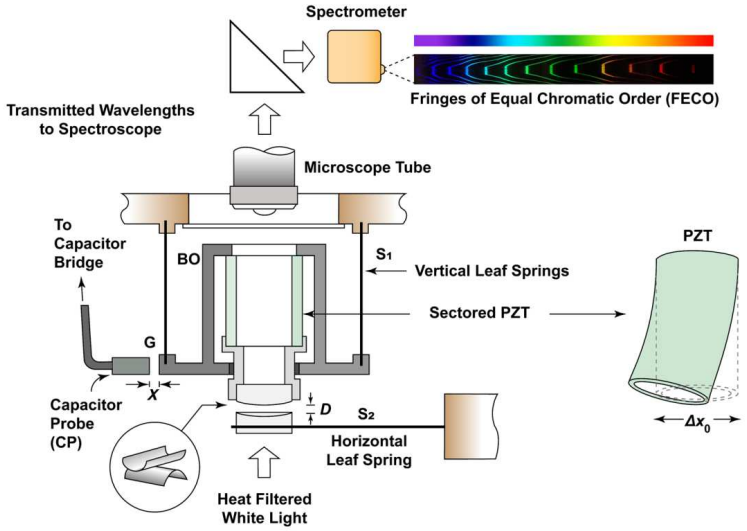

Figure 1. A schematic of a surface force balance used to measure normal and shear forces between two equally thick mica surfaces directly, optimized in particular for measuring weak shear forces. The two back-silvered mica sheets (*ca*. 10 × 10 mm^2) are mounted on fused silica cylindrical lenses in a crossed-cylinder geometry, equivalent to a sphere-plane geometry (as shown in the inset). The absolute separation D between them is calculated via fringes of equal chromatic order (FECO, top right schematic) arising from multiple-beam interference of heat-filtered white light passing through the surfaces. The top lens is mounted on a sectored piezoelectric tube (PZT, magnified on the right to illustrate the sideways motion induced when opposing sectors experience equal and opposite potentials). The PZT is mounted via a rigid stainless-steel boat onto two vertical copper-beryllium leaf springs S_1 which are rigidly mounted into the main body of the balance. The bending of the vertical leaf springs S_1 changes the thickness X of air gap between the boat and a capacitance probe and can be measured with a capacitor bridge, this yields the shear force between the surfaces. The bending of the horizontal leaf-spring S_2 (on which the bottom lens is mounted) is determined by

monitoring the changes in the wavelength of FECO, to yield the normal forces. Reproduced from Klein *et al*., J. Chem. Phys., **108**, 6996 (1998), with the permission of AIP Publishing.

It is appropriate to emphasize three main advantages of the SFB in measuring surface interactions when compared with tip-based methods based on scanning probe microscopy (SPM), such as atomic force or friction force microscopy (AFM or FFM).[28-31] The first is that it directly measures the absolute separations D of the interacting surfaces, while scanning probe methods (including colloidal-force microscopy when the AFM tip is replaced by a colloidal particle[32,33]) measure only the relative separations of the surfaces. A crucial feature of the absolute measurement of D is that contamination of the surfaces, if present, can be unambiguously detected during the normal force profile measurement by comparing with bare surface values.[34] The second is that SFB can measure both shear and normal stresses with a resolution and sensitivity that is some 10^3-10^4-fold (relative to tip probe) or 10^1-10^2-fold (relative to colloidal probe) better than AFM. One limitation for SFB is that particular care is needed in preparing clean and molecularly smooth mica surfaces and mounting them in the SFB. A third advantage of using SFBs is that it is frequently possible to image with high resolution, using AFM or scanning electron microscopy methods (SEM or cryo-SEM) the detailed surface structure of surface attached species, for example surfactant or vesicle layers.[35-47] Such measurements are difficult if not impossible to carry out on the surfaces of colloidal or smaller-sized probes, and together with the SFB force measurements provide considerable additional insight into the origins of the surface interactions. The detailed history and different generations of SFB has been reviewed elsewhere.[48] Here, we will examine progress over the past decade or so using such direct force measurements. We attempt to provide a broad overview of the many different direct surface forces studies, both normal forces and shear or frictional forces, but at the same time focus

in more details on those we feel have provided the most general advances (for example in instrumentation) or physical insights, while clearly aware that such an approach reflects our own view as to their relative importance. These will include the use of different substrates as the test surfaces, including metallic ones, and the effect of changing surface potentials enabled by the use of conducting substrates; recent insights into the properties of highly-confined liquids; interactions between surface-attached polymeric and macromolecular films; and interactions between self-assembled layers of surfactants and lipids, in particular the relevance of the latter to biolubrication processes.

II. Beyond mica - surface forces between different substrates

Mica is a chemical inert, highly crystalline, layered aluminosilicate mineral that can be manually cleaved to obtain thin (1-5 μm) and atomically smooth step-free facets over macroscopic dimensions (~ cm^2).[49] In most of the SFB studies, the substrate is limited to transparent, large areas of atomically smooth mica s§urfaces (or those areas coated with different molecular species). However, mica is a poor conductor of electricity and therefore its surface electrical potential cannot be actively and reversibly controlled. In contrast, a wider range of scientific questions related to interfacial forces would be accessible if the potential of the surfaces could be controlled.[50-56] An efficient way to address this is to cover one of the lenses with polarizable materials instead of mica, typically a smooth metal surface; a major constraint in this case is to ensure that such a metal surface retains a smoothness comparable with the resolution in measuring *D*, that is, a few Ås. In early work, Vanderlick and co-workers[57] created gold surfaces of suitable smoothness (ca. 4 Å rms roughness) through a form of template-stripping, but these were very small (40 μm diameter) which limited their exploitation in

the SFB. A breakthrough came with the work of Chai[58] who, by optimizing the template-stripping approach, was able to create large area (cm^2) gold surfaces with ca. 2Å rms roughness over their entire area for mounting on one of the lenses in the SFB. Chai was also the first to describe a 3-electrode configuration using such a smooth gold surface in the SFB.[59] Both the template-stripping (TS) method and the 3-electrode configuration were used in many subsequent studies where the effect of potential on the surface forces or other surface properties was measured directly. The template stripping was carried out as follows (schematically shown in figure 2). First, as in the traditional procedure of mica preparation,[34] the mica sheets (templates) are placed on a mica backing sheet with fresh exposed facing up, and a thin layer of gold is evaporated onto this smooth template surface. An appropriate area of the template is cut with a scalpel blade, glued onto a lens (gold facing the glue), and stripped away from the gold using a tweezer. The TS process has been used to prepare a wide range of surfaces, including gold,[60-62] platinum,[63,64] palladium,[64] silver,[65] aluminum,[66] and iron.[67] Using the Chai template-stripping method[58] and what they call an electrochemical surface forces apparatus, schematically shown in figure 3a, Valtiner *et al*.[68] showed that confined electric double layer (EDL) forces can be modulated in situ by electrochemical potential variation between a molecularly smooth positively charged amine-terminated surface and a molecularly smooth gold electrode in pH=3. The result (as shown in figure 3b) shows a long-range EDL force which is attractive for electrochemical potentials below the point of zero charge (PZC) and repulsive above the PZC.[69] This interfacial force profile is consistent with standard EDL models. At separation distance below 2 nm (at positive polarization of the gold), the force in figure 3b indicates an additional exponential repulsive force contribution due to hydration forces arising from the confinement of hydrated counter-ions between the two similarly charged surfaces. They also measured the changing

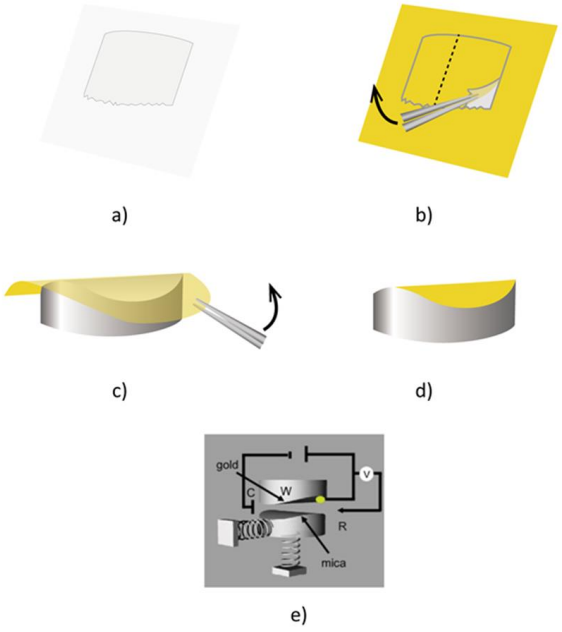

Figure 2. Schematic illustration of the sample preparation and the template stripping (TS) procedure, its mounting, and the three-electrode configuration in the SFB, enabling force measurements between surfaces at controlled potentials. a) The mica is cleaved into 3-6-µm-thick facets (thinner mica sheets are hard to strip away from the gold, while thicker ones are difficult to attach affinely to the curved lens through capillary attraction by the molten glue). The pieces are then placed on a mica backing sheet with their freshly exposed part facing up. b) A thin layer of gold film is slowly evaporated using an e-beam on the mica. Following evaporation, the sample is annealed for 2 h. An appropriate size of mica piece is cut with a scalpel blade and lifted from the backing sheet by a tweezer with extreme care. c) The lifted gold-coated mica piece is glued using epoxy onto a cylindrical fused silica lens with the gold facing the glue. The mica is then gently stripped off using a tweezer (enabled by weak adhesion due to the lattice mismatch between gold and mica). d) A smooth gold surface on the lens, mimicking the mica template surface, is exposed. The lens is rapidly mounted and covered with water in the SFB within 1 min of exposure. (e) shows the three-electrode configuration, with the platinum counter-electrode C, the gold working electrode W and the silver quasi-reference electrode R. (a) – (d) reproduced with permission from Chai *et al*., Langmuir **23**, 7777 (2007). Copyright 2007, American Chemical Society. (e) reproduced with permission from Chai Liraz Ph.D thesis. Copyright 2007, Weizmann Institute.

thickness of growing oxide layers on the gold surfaces when the electrochemical potentials were above the oxidation potential (as shown in figure 3c). Later on, Shrestha *et al*.[64] extended the

technique to platinum and palladium, and visualized dynamic processes including electron transfer, oxide reduction/oxidation, and solution side reaction at electrochemically active metal interfaces in real-time within the SFB. In contrast to the Valtiner studies,[64,69] it is possible to adjust the gold potentials within a range of values where oxidation and reduction at the surface are negligible, so that the gold electrode is ideally polarized and no faradaic current flows. Tivony *et al*.[70] worked under such 'ideal' conditions to measure directly the forces between a mica surface and the gold surface at different externally-applied potentials; they were able to show directly for the first time a confinement-induced surface-charge inversion at the metal surface. In a separate study,[71] Tivony *et al*. exploited the fact that out-of-equilibrium electric double layers at the surfaces generate significant transient forces that may be much larger, particularly at values of $D >> \lambda_D$, the Debye screening length at the relevant salt concentration, than van der Waals and double layer forces. Using an SFB with a three-electrode configuration between a single-crystal mica surface and a smooth gold surface prepared by the Chai template-stripping method[58] (as shown in figure 4a and 4b), they exploited such transient forces, while stepping the potential, to measure directly the EDL charging of a nanopore between the surfaces. Similar nanopores are central elements of various high-capacitance devices used in different applications refs.[72-74] Figure 4c shows the transient surface-separation change during potential steps between + 200 mV and – 200 mV at surface separations at D = 50 nm. In response to abrupt potential steps, an electrostatic force (F_e) exerted from an unscreened electric field, which bends the spring by ΔD over a time Δt_s. As counter-ions redistribute in the EDL (charging) within the nanopore, F_e gradually decreases and the surfaces

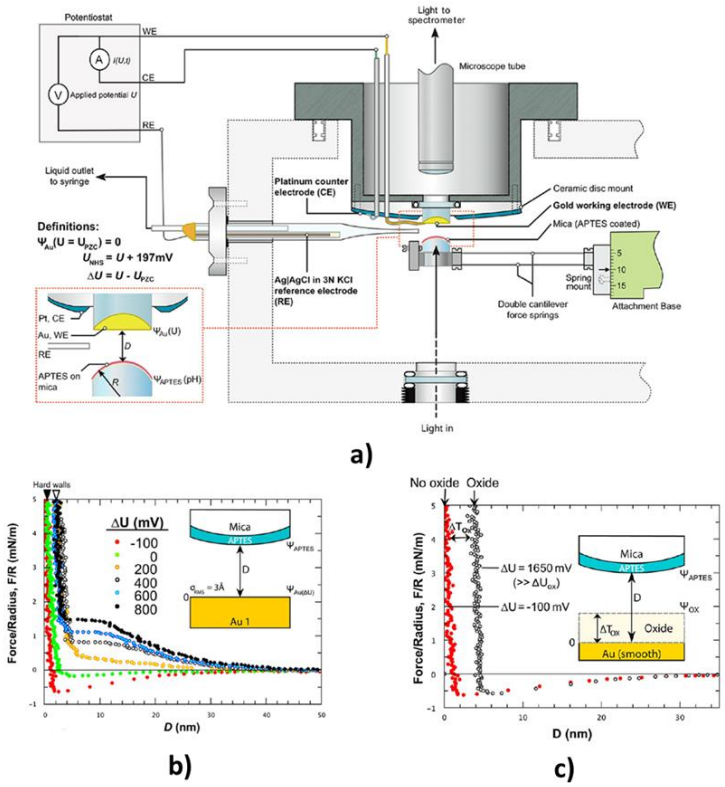

Figure 3. Schematic of the electrochemical three-electrode configuration used in the electrochemical surfaces forces experiments[69,75-78] and the typical force-distance profiles. a) This setup consists of a working electrode (WE) that defines the studied interface, a counter electrode (CE) that supplies the electrochemical current required by the WE, and a reference electrode (RE) that maintains at a constant reference potential. b) Typical force-distance profiles measured during approach of the atomically smooth gold surface and positive charged (3-aminopropyl)-triethylsilane (APTES) coated mica surfaces measured as a function of the externally applied electrochemical potentials. c) Typical force-distance profiles measured during approach of the gold and APTES coated mica surfaces measured at high anodic externally applied electrochemical potentials that are higher than the oxidation potential, where the gold surface oxidizes. Reproduced with permission from Valtiner *et al*., Langmuir **28**, 13080 (2012). Copyright 2012, American Chemical Society.

relax over a time Δt_r (as shown in figure 4d). This study found that the nanopore charging time is order of a second, which is far slower than the time for charging an unconfined surface (typically

order of 10^{-2} s), increasing at smaller pore sizes, and decreasing with higher ion concentration. The results are the first direct determination of the charging dynamics of an individual nanopore, and are consistent with the classic transmission line model applied to the nanopore geometry.[79-81]

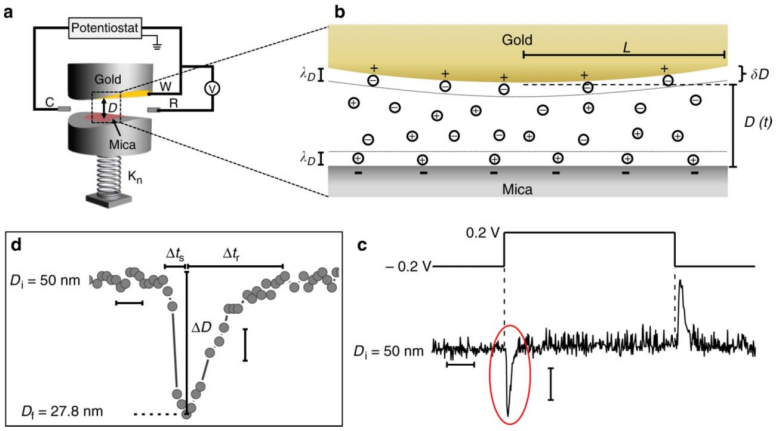

Figure 4. Electric double layer charging dynamics within a single nanopore studied by a surface force balance. a) Schematic of the surface force balance with a three-electrode configuration between a single-crystal mica surface and a smooth gold surface (root-mean-square roughness ca. 3 Å) at a controlled potential. b) A section through the intersurface gap at closest separation D, showing its nano-slit like structure, where λ_D is the Debye length, L is the radius of the circular pore, δD is the change in pore width at a distance L from the pore center due to curvature of the surfaces ($\delta D \approx L^2/2R$). The schematic is not to scale: L is typically 100 μm and D is of order 100 nm. c) A dynamic measurement of D(t) trace taken in 5 mM $NaNO_3$ (λ_D = 4.3 nm) at D = 50 nm (>> λ_D) based on video recording of the motion of the interference fringes[52,70] (reflecting the movement of the lower mica surface), in response to positive (– 0.2 V→+ 0.2 V) and negative potential (+ 0.2 V→ – 0.2 V) steps as indicated by the upper potential trace. Scale bars: horizontal – 2 s; vertical – 10 nm. d) An asymmetric shape of D(t) plot (enlarged from the red circled peak in (c)) due to the ion migration into a charging nanopore, where Δt_s and Δt_r signify the initial motion and relaxation time, and ΔD is the distance shift from initial surface separation D_i = 50 nm to extremal separation D_f = 27.8 nm. Scale bars: horizontal – 0.2 s; vertical – 5 nm. Reproduced with permission from Tivony *et al*., Nat. Commun. **9**, 4203 (2018). Copyright 2018, Nature Publishing Group.

Graphene is an allotrope of carbon consisting of a single layer of atoms arranged in a two-dimensional honeycomb lattice; it is a transparent and flexible conductor that holds great promise

for a broad range of applications, including electronics, membrane-separation technologies, energy, and medicine.[82-84] In a promising extension to new substrate materials for surface forces measurements, Perkin and co-workers[85] reported a method for creating exceptionally smooth graphene layers (root-mean-square roughness of 0.19 nm) over large areas (> 1 cm^2), and a means of adapting the SFB to use such layers as model substrates, as shown in figure 5. The graphene SFB (gSFB) measurements under aqueous electrolyte solution revealed EDL forces down to nanometer separation between two smooth graphene sheets; as graphene is a conductor, normal forces at variable externally-applied potential control could be investigated.

In view of the paucity of methods to characterize the surface energies of two-dimensional materials refs,[86,87] such as graphene, it is notable that van Engers *et al.*[88], using the gSFB, reported the first direct measurement of the interfacial energy (γ) of CVD graphene using both single and few-layer graphene under dry conditions, as well as under water and sodium cholate. With the SFB this is readily achieved by measuring the force $F_{\text{pull-off}}$ required to separate the surfaces from adhesive contact, which can be directly related to the surface energy γ according to the Johnson−Kendall−Roberts (JKR) relation,[89]

$$\gamma = \frac{F_{\text{pull-off}}}{3\pi R} \qquad (1),$$

where R is the radius of the curvature of uncompressed surfaces. Thus, the gSFB provides direct insight into surface interactions of 2D-materials, with the possibility of investigating surface forces between these materials across liquids and under different applied surface electric potential. Of particular interest may be the frictional interaction between two graphene layers in the gSFB, as a function of their lattice mismatch angle, in view of the recently-discovered properties of such layers

at 'magic-angle' mismatch[90,91] together with the possible relation between their electronic properties and their frictional dissipation as they slide past each other.[92,93]

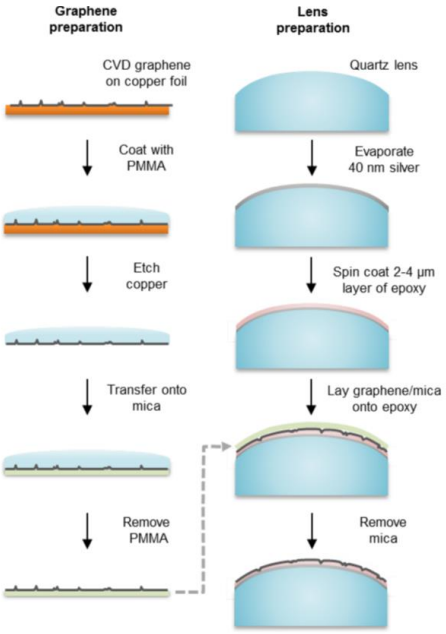

Figure 5. Schematic of the surface attachment of graphene onto mica for the gSFB, enabling force measurements with a different substrate. (Left) Transfer of chemical vapor deposition (CVD) graphene onto the mica template by polymer-based transfer methods. Following CVD growth of graphene on copper, the graphene is coated with poly(methyl methacrylate) (PMMA). After etching, the copper is removed and the graphene/PMMA is placed onto the freshly cleaved mica. Finally, PMMA is removed with anhydrous acetic acid. (Right) Preparation of SFB lens with the ultraflat graphene surface. A total of 40 nm of silver is evaporated onto the SFB lens. Subsequently, the graphene/mica stack is glued onto an SFB lens with a spin-coated epoxy coating (2-4 µm). Upon removal of the mica template in water a clean, smooth, graphene surface is exposed without` positive protrusions. Reproduced with permission from Britton *et al.*, Langmuir **30**, 11485 (2014). Copyright 2014, American Chemical Society.

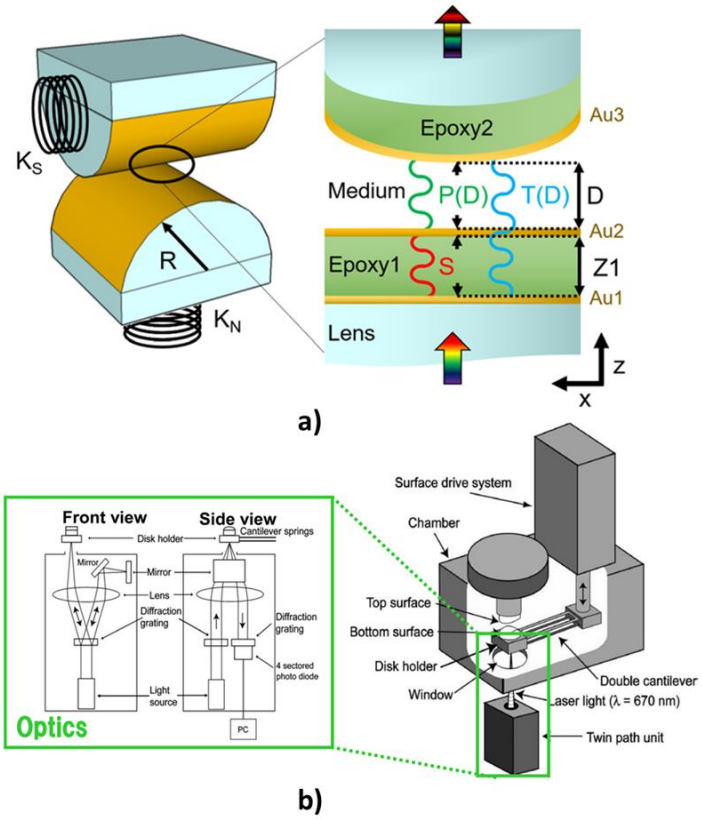

Figure 6. Schematic of two types of SFBs for the force measurement between two metallic and reflecting surfaces. (a) Left: schematic of the 3-mirror SFB setup using gold as the mirror material.[94] The gold-coated lenses are placed in crossed-cylinder configuration, equivalent to a sphere on a flat surface. Normal and lateral forces are measured by monitoring the displacement of the surfaces mounted on shear-force and normal-force springs with known spring constants (K_S and K_N) with respect to a known applied motion. Right: light enters the setup, constructively interferes between the different mirrors, and emerges as an interference pattern. Primary fringes [P(D), shown in green] depend on the distance between the mirrors (D) and originate from reflections between mirrors Au2 and Au3, across the medium. Secondary fringes (S, shown in red) are distance independent and arise from reflections between mirrors Au1 and Au2, across the epoxy spacer with thickness Z1. Distance dependent tertiary fringes [T(D), shown in blue] arise from reflections between mirrors Au1 and Au3. By combining these the separation D between Au2 and Au3 may be evaluated (b) Schematic of the twin-path surface forces apparatus for opaque substrates and/or nontransparent fluids ref.[95] Right: Laser light goes through the window at the bottom of the chamber and is reflected by the

back of the disk holder. The reflected light is monitored by the twin-path unit. The surface distance is controlled by a surface drive system. Left: Front view and side view of twin path displacement measurement unit. The beams separated by the diffraction grating are reflected by the bottom of the disk holder and by the fixed mirrors, respectively. They are then recombined on the diffraction grating in the front of the four-sectored photodiode that monitors the recombined and phase-shifted light. The signals reaching the photodiode are analyzed with a computer to yield the relative displacements. For (a), reproduced from Van Engers et al., Rev. Sci. Instrum. 89, 123901 (2018), with the permission of AIP Publishing. For (b), reproduced with permission from Kurihara *et al*., Langmuir 32, 12290 (2016). Copyright 2016, American Chemical Society.

It is often of interest to measure forces between two polarizable surfaces, and while the gSFB[85] in principle provides such a possibility, using two metallic surfaces – for example two template-stripped metal films as described above[58,63,96-98] – enables to probe a much wider range of surface properties. In the conventional SFB approach, the force measurement between two such metallic and reflecting surfaces facing each other with no spacers is complicated when employing FECO, since interference maxima – from which the value of D is extracted – are not possible when the optical path difference between the surfaces is below the diffraction limit.[94,99] Likewise when the interacting surfaces are opaque the FECO approach is not possible, and various SFB configurations to by-pass this limitation were proposed.[29,95,100] Other types of SFBs designed for measuring surface forces between opaque substrates have been further limited by shortcomings such as short working distance,[101] working with non-polar liquids only,[102] and difficulty in handling the bimorph sensors.[103] Based on the 3-mirror approach originally proposed by Levins *et al*.,[104] van Engers *et al*.[94] recently developed a simple technique for the fabrication of uniform epoxy layers, amenable to producing a 3-mirror configuration with two template stripped gold surfaces (as shown in figure 6a). This setup allows for surface force measurements across confined electrolytes with potential control of both ultra-smooth, directly-interacting electrode surfaces (Au2 and Au3 in figure 6a). A different approach, twin-path surface force measurement (schematic shown in figure 6b) was

developed in Kurihara's group for interactions between two opaque substrates and/or in nontransparent liquids, including electrochemistry using two opposing metal electrodes as substrates,[63,97,98] and characterizing surface interactions between ice and other substrates.[105,106] However, unlike the 3-mirror method,[94] this twin-path approach doesn't measure the absolute surface separation since it uses the hard wall contact as the zero distance, and additionally loses optical information, such as the radius and continuity of the contact area.

III. Strongly-confined fluids

The properties of highly confined liquids – as they differ from those bulk liquids – are both of basic interest, and also play a role in a wide range of effects of practical interest, from tribology to the stability of nanoparticulate dispersions. Here we note some of the notable advances over the period covered by this review.

3.1 Organic liquids

Many studies have been reported on a variety of ultrathin organic liquid films confined between two surfaces, ranging from nonpolar linear alkanes, such as *n*-decane and *n*-dodecane,[107,108] cyclic molecules, such as octamethylcyclotetrasiloxane (OMCTS),[5,27,108-112] to molten salts such as ionic liquids.[113-117] At confinements down to molecularly thin films (*ca*. 5-8 molecular layers) between smooth mica surfaces, organic liquids become solid-like, which may be interpreted in terms of their densification near the confining walls[118,119] and the fact that for such organic materials the solid phase is denser than the liquid phase, while the unconfined liquids remain disordered and fluid at the same conditions.[31] Earlier work had shown that for the case of quasi-spherical molecules such as cyclohexane and OMCTS the transition between fluid and solid-like behaviour could be abrupt

and occur over additional confinement by a single molecular layer, as illustrated in figure 7a, b,[109,120] while shear of such confinement-solidified liquids often occurred via stick-slip motion, as indicated in figure 7c.[20,21,110,121-124] The mechanism of such stick-slip sliding was believed to be due to intermittent shear-melting and solidification of the sheared, confined liquid,[27,125,126] while understanding the molecular origins of such stick-slip – which in macroscopic systems may lead to increased friction and wear relative to smooth sliding[122,127-130] – could lead to improved lubrication strategies. In the shear-melting scenario, the shear-induced solid to liquid transition at the point of stick to slip should be associated with a dilation of the confined film due to the density decrease as the solid phase is fluidized.[131] Rosenhek-Goldian *et al*.[132] confined an OMCTS film between mica surfaces in an SFB, and monitored the film thickness during stick-slip sliding via fast video recording. Using data-analyzing tools from classical signal detection theory to correlate the slip events with the instantaneous value of the film thickness (as indicated in figure 7d), they demonstrated experimentally for the first time that no dilation of the sheared film occurred at the transition from stick to slip, down to the 1Å level. Since a dilation of ca. 3-5Å (depending on the film thickness) is expected from an ~10% density decrease in the OMCTS film arising from its shear melting, this absence of dilation (within the system resolution of 1 Å) showed clearly that no shear melting occurred at the stick-to-slip transition. Rather, Rosenhek-Goldian *et al*. suggested that other modes, such as interlayer or wall slip rather than shear melting, may be the dominant energy dissipation modes on shear of the OMCTS film, a suggestion subsequently supported by a detailed molecular dynamic simulation.[133]

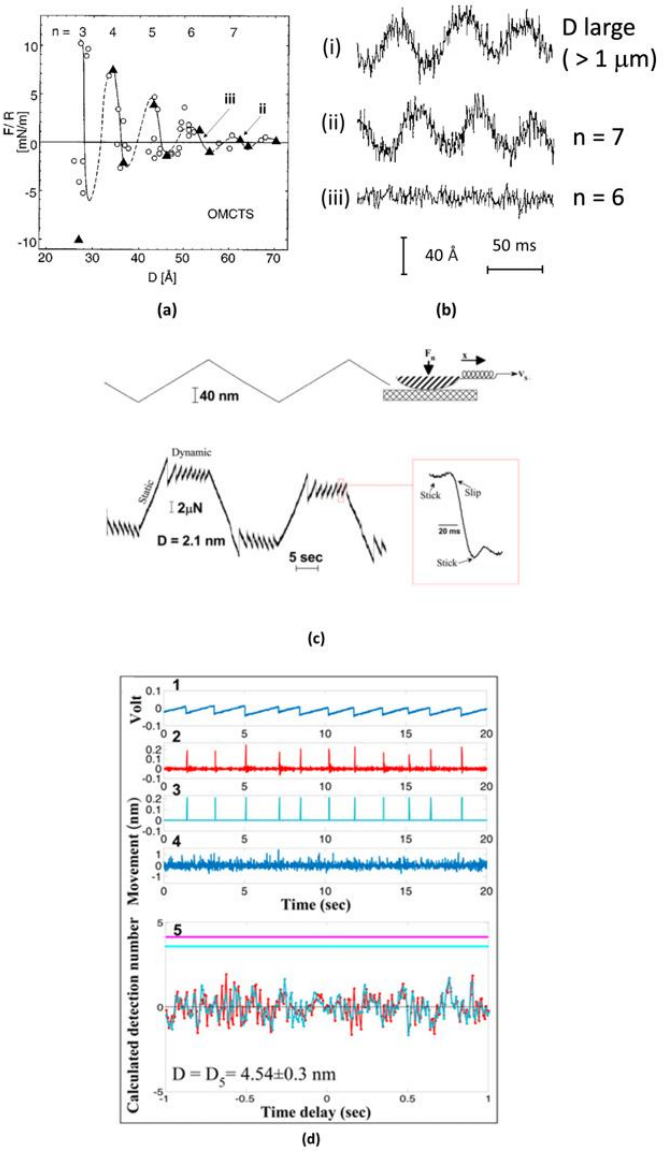

Figure 7. Illustrating confinement-induced solidification of organic liquids and testing the idea that stick-slip across such solidified OMCTS is a shear-melting effect. (a) Force distance profile between curved mica surfaces immersed in OMCTS,[109] showing oscillations, with each maximum

corresponding to the number of monolayers n. (b) Shear motion traces for the mica surfaces across OMCTS. These show that as the film is progressively confined from large separations (trace (i)), the oscillations arising from ambient noise shear the still-fluid OMCTS at 7 monolayers, point (ii), but are frozen out when the OMCTS solidifies as it is confined to 6 monolayers, at point (iii). (c):Top trace is the lateral back and forth motion applied to the top mica surface across OMCTS at a surface separation $D = 2.1 \pm 0.2$ nm ($n = 3$) at v_s via the shear spring as indicated in the schematic on the right. Bottom trace is the shear force corresponding to the bending of the shear spring. A characteristic stick–slip sliding pattern is seen, with the inset showing a single slip event, of duration *ca*. 20 ms, on an expanded time scale, (d) Correlation of slip events, during stick–slip sliding across OMCTS films of thickness D, with changes δD in gap separation. Plot 1 shows the stick–slip sliding trace across a $D = 4.5 \pm 0.3$-nm-thick OMCTS film ($n = 5$). Plot 2 is the natural signal, for these control experiments, obtained by applying sampling rate conversion and normalization to the signal. Plots 2 and 3 identify the stick-to-slip transitions to correlate with the actual values of δD determined via fast video recording during the period of the applied displacements, plot 4. Plot 5 shows the correlation between the stick-slip transitions and δD; taken from ref.[132]. The point of (d) is that it shows an absence of any correlation of the slip events with dilation δD (at any level above 1Å) of the sheared OMCTS film; thereby demonstrating that shear melting does not occur at the stick-to-slip transition. Any such correlation would have resulted in a peak in plot 5 of magnitude at least equal to the horizontal turquoise line.[132] For (a) and (b), reproduced from Klein *et al*., J. Chem. Phys., **108**, 6996 (1998)ref.28. Copyright 1998, American Institute of Physics, with the permission of AIP Publishing. For (c) and (d), reproduced with permission fromRosenhek-Goldian *et al*., Proc. Natl. Acad. Sci. **112**, 7117 (2015). Copyright 2015, National Academy of Sciences.

In a different SFB study, Smith *et al*.[134] investigated the effect of relative crystal orientation on the friction across molecularly-thin confined dodecane films. Under dry conditions, when the two surfaces are crystallographically-aligned ($\theta = 0^0$) the commensurabilty of the two mica surfaces is transmitted across the confined dodecane and thus large frictional dissipation is seen, while at $\theta = 90^0$ the incommensurability of the lattices greatly weakens the lateral ordering of the confined molecules and thus reduces the frictional force (as shown in figure 8). This study resolves earlier dissonance between the results obtained by different groups concerning the nature of the phase-state (liquid-like or solid-like) of highly-confined lubricant layers, and the nature of the frictional dissipation modes as the confining compressed surfaces slide past each other.[126,135,136] More

importantly, it makes the first clear connection between friction involving thin lubricant layers and structural superlubricity between incommensurate surfaces.[137]

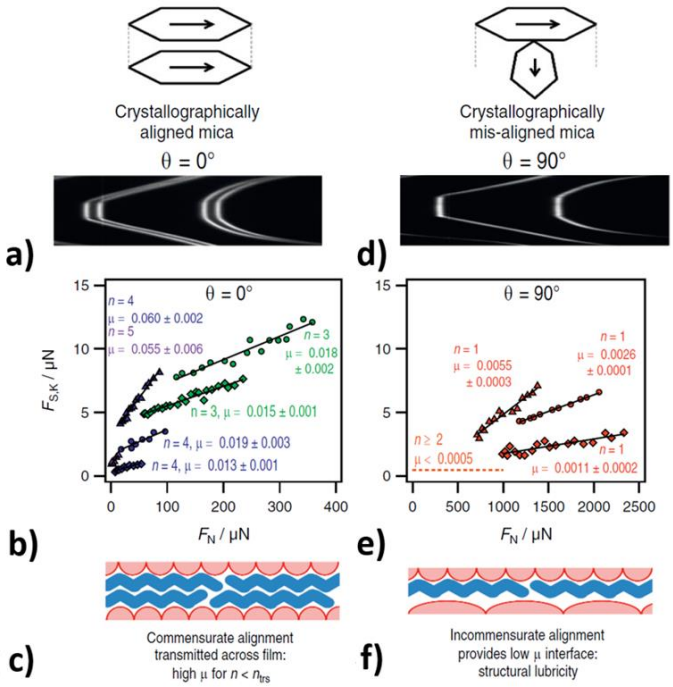

Figure 8. Confinement-induced solidification with structural ultralow friction between surfaces made incommensurate by modifying the alignment of the opposing mica substrates. Comparison of friction measurements carried out with dodecane films between two mica surfaces mounted (a-c) in relative crystallographic alignment, $\theta = 0^0$, and (d-f) in crystallographic misalignment, $\theta = 90^0$. (a) and (d) show typical FECO patterns for aligned (doublets fringes) and misaligned (singlets fringes) surfaces. (b) and (e) show kinetic frictional force $F_{S,K}$ versus F_N between two mica surfaces across the thin film for a range of different n (number of layers). (c) and (f) are the schematics to illustrate the interpretation, as described in the text: A laterally ordered dodecane film can sit in commensurate alignment with the mica surface, transmitting the mica crystalline symmetry into the film. In the case where the two mica sheets are crystallographically aligned (in c), the solidified and two-dimensional ordered dodecane film can cause the surfaces to "lock" together, and the junction exhibits higher friction. Conversely, when the mica sheets are misaligned (in f), such that their

lattices are incommensurate, the dodecane film can only align with one (not both) surface, and there must always exist at least one interface of lattice mismatch and therefore low friction. Reproduced with permission from Smith *et al*., Proc. Natl. Acad. Sci. **116**, 25418 (2019). Copyright 2019, National Academy of Sciences.

Thanks to the unique properties of room temperature ionic liquids (ILs), namely their low vapor pressure, high thermal stability, controlled miscibility, and high electrical conductivity, they have many potential applications, including acting as powerful solvents,[138] electrolytes in energy storage devices,[139,140] lubricants,[141,142] and others.[143,144] Under nanoscale confinement structural forces are identified for different protic and aprotic ILs, arising from their layering adjacent to the solid substrate;[113,117,145] similar to those seen for non-polar liquids as noted earlier. The main difference between the structural forces observed for non-polar liquids and ILs is that each oscillation in force corresponds to the squeeze-out of one molecular layer, whereas the oscillation period for ILs is comparable to the size of an ion-pair layer (one cation layer and one anion layer) as required to maintain electroneutrality. Due to the strong interaction between ILs and solid surfaces, arising from their unique dipolar nature,[54,146-149] it has been observed that ILs are very difficult to squeeze outfrom between confining surfaces even under high pressure,[145] while less polar molecular lubricants are adsorbed to the surfaces largely by van der Waals interactions, and so may be removed more easily.[109] This ability to form robust boundary layers which resist squeeze-out makes ionic liquids potentially good lubricants, and indeed in the past two decades ILs have emerged as potential alternatives to replace traditional lubricants.[150] The shear behavior of ILs under confined geometries has been extensively investigated using SFBs.[117,123,124,151-155] In contrast to most molecular liquids, the friction coefficients correlate with the number of ILs layers confined between the surfaces ('quantized' friction),[123,152] (early evidence of such correlation was seen also for highly confined

organic liquids including cyclohexane and OMCTS[27,156]). This is seen in figure 9a, where friction was measured across the IL 1-butyl-1-methylpyrrolidinium bis(trifluoromethylsulfonyl)imide,

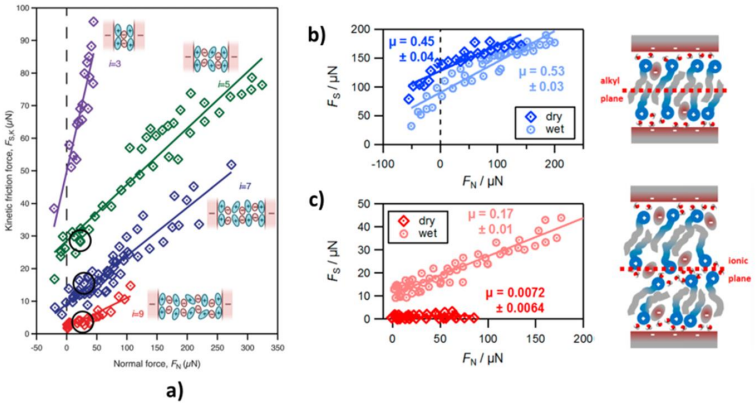

Figure 9. Quantized friction and molecular friction mechanisms across ionic liquid thin films. (a) Shear or frictional force $F_{S,k}$ *vs*. normal load F_N measured in the SFB across $[C_4C_1Pyrr][NTf_2]$ for different numbers of ion layers, i, in the film. The lines are linear fits to the data. Inset cartoons indicate the liquid structure for each regime. F_S *vs*. F_N measured in amphiphilic $[C_{10}C_1P_{yrr}][NTf_2]$ for one (b) and two (c) bilayers; the friction across one bilayer is shown in blue and schematic of the one bilayer structure on the right; the friction across two bilayers is shown in red and schematic of the two bilayers structure on the right. Lines are linear fits to data from four experiments using different pairs of mica sheets. The diagrams indicate the active planes of shear (labeled with red dashed lines). For (a), reproduced with permission from Smith *et al*., Phys. Chem. Chem. Phys. **15**, 15317 (2013). Copyright 2013, Royal Society of Chemistry. For (b) and (c), reproduced with permission from Smith *et al*., J. Phys. Chem. Lett. **5**, 4032 (2014). Copyright 2014, American Chemical Society.

$[C_4C_1Pyrr][NTf_2]$ for different numbers of ion layers, each corresponding to a different linear friction-load relationship. The variation of the zero load friction can be understood as the adhesion contribution, which increases as the number of layers in the film decreases.[5,117] ILs with sufficiently amphiphilic cations can self-assemble to form lamellar cation bilayers in confinement.[157,158] Under such conditions, shear could occur at the ion/mica interface, between the alkyl chains of the bilayers,

or within the ionic region between bilayers. To answer this question, Smith *et al*.[152] measured friction between atomically smooth, negatively charged mica surfaces across molecularly thin films of amphiphilic 1-decyl-1-methylpyrrolidinium bis[(trifluoromethane)sulfonyl]imide, $[C_{10}C_1Pyrr][NTf_2]$ for one and two bilayers of this IL, both with and without the addition of small amounts of water. A key finding of this study is that the friction coefficient for a single bilayer is independent of the water content (as shown in figure 9b), whereas it increases by more than an order of magnitude for two bilayers when water is added (as shown in figure 9c), an effect attributed to an increase in order of the ions within the shear plane.[151,159] These implications indicate the subtle energy dissipation mechanisms at play in systems of one and two bilayers. Most significantly, a film of lubricant thick enough to contain two (or more) bilayers will shear along the ionic planes rather than at the alkyl planes, and the friction coefficient of these planes can be orders of magnitude lower than that for a single confined bilayer. There are two major differences between the frictional responses of ILs and non-polar liquids: First, the friction coefficient with ILs is quantized and increases monotonically when the number of layers decreases,[123,152] while for non-polar liquids variation of friction coefficient with number of layers may be much smaller.[27] Secondly, friction coefficient values can be much lower for ILs than for non-polar molecules. This relatively low resistance to shear together with the ability to resist squeeze-out makes ILs promising lubricants.

3.2 Aqueous systems

In contrast to non-associating liquids, whose viscosity increases by many orders of magnitude when they are confined down to a few layers, SFB measurements showed that pure water remains fluid with a viscosity close to its bulk value, even when confined to films as thin as one monolayer.[160]

PLEASE CITE THIS ARTICLE AS DOI: 10.1063/5.0059893

This unusual behavior may be attributed to the different phase density behaviour for water compared to most non-associating liquids, where its solid phase is less dense than liquid water (i.e. ice floats). Thus the densification of the water within the gap due to its attraction to the confining walls suppresses its tendency for solidification.[161,162] This persistent fluidity under strong confinement of pure water may be modified in the presence of salt ions. Metal cations, especially those of the alkali series Na^+, K^+ etc, which are ubiquitous also in biological systems, but also multivalent ions, are strongly hydrated due to their charge interacting with the large water dipoles, and surrounded by hydration shells. When salt solutions (above a certain critical concentration) are confined between mica sheets in the SFB, hydrated metal counterions are trapped between the negatively-charged mica surfaces, resulting in a strong so-called hydration repulsion between them, as is long known.[13,14,163] Using an SFB, Raviv *et al*.[15] discovered that two mica surfaces strongly compressed down to sub-nanometer separations across NaCl solutions in the hydration-repulsion regime could slide past each other with extremely low friction. They attributed this[15,164] to the extreme fluidity of water molecules in the hydration shells, combined with the difficulty of squeezing them out from between the compressing surfaces (owing to the large energy penalty associated with the increase in the bare-ion self-energy). This combination results in a striking reduction in friction (as shown in figure 10b) when two surfaces slide past each other, and is termed hydration lubrication.

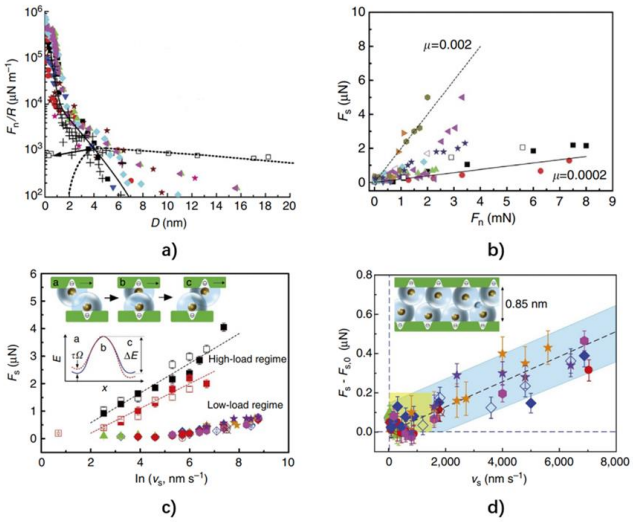

Figure 10. Probing the origins of hydration lubrication by shearing confined hydrated ions between atomically smooth mica surfaces. (a) Normalized force profiles $F_n(D)/R$ versus surface separation D between mica surfaces, across 0.1 M sodium salt solutions. Empty squares are the control pure water profile, with arrow indicating jump into adhesive contact, while other different symbols correspond to different contact points, including different experiments. The solid lines are a fit to a Derjaguin-Landau-Vervey-Overbeek (DLVO) expression, together with a short-ranged exponential term. The dotted line for the pure water control is a fit to the DLVO expression. (b) Summary of F_s versus F_n data, at sliding velocity v_s = 200 nm s^{-1}. The lines correspond to friction coefficients μ as indicated. (c) Variation of F_s with v_s, in both high- and low-load regimes. Shown are data at two high loads (black and red squares, F_n = 6-8 mN) for which the surface separation D = 0.48±0.15 nm; and at several low loads (all other symbols, F_n = 0.1-0.2 mN) for which D = 0.85±0.15 nm. The variation in the high-load regime, straight broken lines, is F_s= A+B·ln(v_s), where A and B are constants. The inset cartoon illustrates the sliding mechanism for the high-load regime. Hydrated ions are localized at the oppositely charged surface sites and must overcome an energy barrier ΔE to move past each other as the surfaces slide. (d) The $F_s(v_s)$ variation in the low-load regime is amplified from (c). The data are plotted as (F_s-$F_{s,0}$) versus v_s. The inset cartoon is for D = 0.85 nm, and illustrates the filling by the hydration water of this intersurface gap. Reproduced with permission from Ma *et al*., Nat. Commun. **6**, 6060 (2015). Copyright 2015, Nature Publishing Group.

Ma *et al*.[164] examined the origin of the hydration lubrication effect by shearing two surfaces across high concentration NaCl, at different separations D and shear rates $\dot{\gamma}$, as shown in figure 10. In the

high-load regime, at surface separations comparable with twice the diameter of the bare Na^+ ions, as in fig. 10c, the sliding may be understood in terms of a rate activated process where surface-localized counterions need to squeeze past each other (figure 10c cartoon). The resulting frictional force F_s varies with sliding velocity v_s as[164,165]

$$F_s(v_s) = (Ak_BT/\Omega)\ln(v_s) + \text{constant} \qquad (2),$$

where A is the contact area, k_B and T are Boltzmann's constant and the absolute temperature, Ω is the stress-activated volume associated with sliding of ions past each other, and the constant is linear in the activation energy ΔE (inset cartoon to figure 10c). In the low-load regime, the surface separation is such ($D \approx 0.85$ nm) that essentially all the water molecules belong to primary hydration shells of the trapped counterions. The energy dissipation on sliding then originates in the shearing of the hydration shells, and from the variation of the resulting shear stress with sliding velocity an effective shear viscosity η_{eff} of the hydration shells may be evaluated. From the slope of the blue band in figure 10d, a value $\eta_{eff} = 0.22 \pm 0.07$ Pa·s is evaluated, which, though it is some 200-fold higher than that of bulk water, still implies a very fluid-like response to shear of the hydration layers surrounding the charges (a similar increase of η_{eff} was seen in molecular dynamics (MD) simulations of pure water confined between polar surfaces at a separation of about 0.3 to 0.4 nm[166]). Hydration lubrication, through shear of hydrated ions or counterions at the interface between sliding surfaces as indicated above has, over the past decade, emerged as a new paradigm and organizing principle for understanding and controlling frictional processes in aqueous media. This is seen in the large number of studies of widely different systems, some of which are described below, where hydration lubrication is an important or central ingredient, ranging from friction reduction in biological environments[167-187] to automotive applications.[188-196] Recent work by Tivony and Zhang[197] using

the SFB, where a smooth metal (gold) surface at controlled potential faces a dielectric (mica) surface at constant charge (as described in the previous section), demonstrated that changes of the metal surface potential could be used to either trap or to expel hydrated ions from between the surfaces. In this way they were able to turn hydration lubrication on and off via an external potential control, an effect that led to readily switchable friction between the surfaces.

Hydration repulsion forces (short-ranged forces of non-DLVO origin as described above) are seen not only between hydrophilic surfaces (such as mica or lipid bilayer surfaces, see below) across aqueous solutions, but may act also between hydrophobic surfaces, and are observed in numerous biophysical phenomena.[198,199] Hydrophobic hydration arises due to interaction of water molecules with anions or cations adsorbed on hydrophobic surfaces.[200-202] Most studies, including spectroscopic experiments,[203] zeta potential measurements,[204] titration experiments,[205] and MD simulations,[206] suggest a solid hydrophobic surface is negatively charged in a neutral or high pH aqueous medium.[207,208] Donaldson *et al*.[208] found that surface interaction between hydrophobic polydimethylsiloxane (PDMS) and hydrophilic mica are fully repulsive at all separations at pH of 10, due to repulsive electrostatic and hydration forces, indicating that the PDMS is negatively charged at high pH. Recent SFB measurements[209] have shown that hydration lubrication can be active between a hydrophilic mica and a highly hydrophobic fluoropolymer film across pure water and 0.1 M NaCl. The monotonic repulsion was due to trapped hydrated counterions (protons and Na^+ ions) between the negatively charged hydrophobic surface and mica. The hydrated trapped ions were not squeezed out even at pressures of up to at least 50 atm, resulting in very low frictional dissipation via the hydration lubrication mechanism. For completeness we note that a net positive

charge at the air/water or oil/water interface - which differs from the solid hydrophobic surface/water interface - has been observed in some studies[210-214] (MD simulations, surface tension measurements, etc.), and attributed to the absorption of hydronium H_3O^+ ions.

In addition to the emergent hydration lubrication mechanism which was discovered through shear force studies, measurements of the normal forces in the SFB across concentrated salt solutions have led to an unexpected new finding. At sufficiently high electrolyte concentrations (typically at concentrations >1 M), a longer-ranged repulsive force of non-DLVO origin has been observed between two mica surfaces (as shown in figure 12a).[215] Instead of a decreasing Debye screening length λ_D which describes the decay with D of the EDL repulsion at increasing ion concentration c in dilute electrolytes, as predicted by classical Debye-Hueckel theory ($\lambda_D \sim (1/c^{1/2})$, the experimental decay length at the highest c values turns out to be much larger than the theoretical Debye value (as shown in figure 11b); this effect was also observed in ionic liquids[147] and in large soft ions solutions.[216] The effect has been theoretically attributed to different origins[217-220] including that the Debye−Hückel theory may not apply when the Debye length becomes comparable to dimensions of an ion.[221] The oscillatory forces region (0−3 nm), which is due to the squeezing out of layers of hydrated ions seen also in the step-features in the force profile (figure 11a), can be well observed in the SFB measurement.[222] Perkin and co-workers also presented a series of SFB results showing that λ_{exp} follows the scaling relationship $\lambda_{exp} \sim l_B c a^3$, where l_B is the Bjerrum length and a is the ion diameter.[223] However, while several theoretical treatments have attempted explain these results, there is not yet a full consensus as to its precise origins.[217-220]

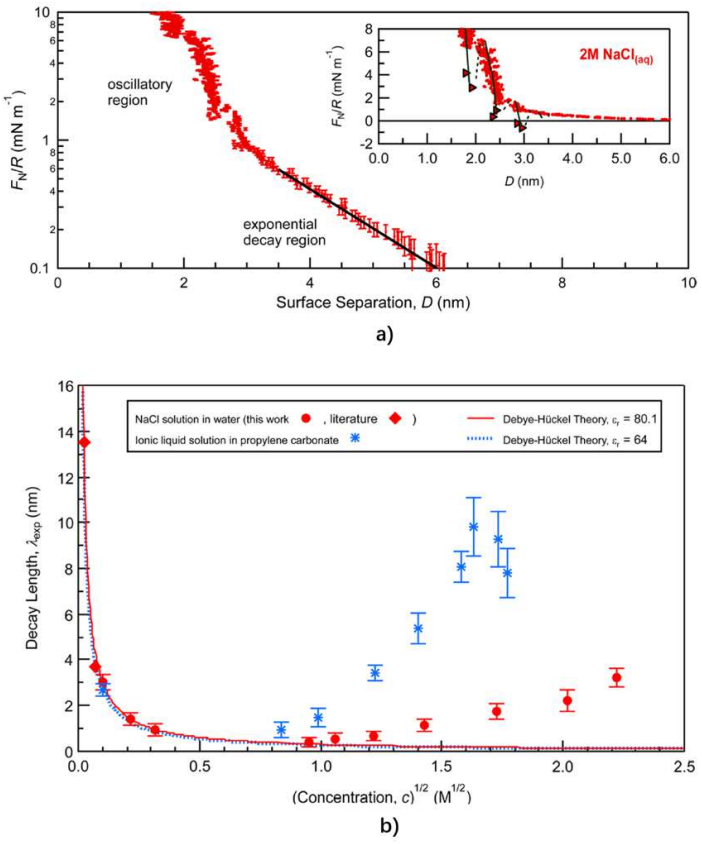

Figure 11. Direct measurements of the force between atomically smooth mica surfaces across concentrated electrolytes show that the electrostatic screening length at high concentrations unexpectedly increases with concentration. (a) Normalized force profiles of F_N/R between versus surface separation D between mica surfaces across 2 M NaCl aqueous solution. The solid line is the exponential fit of the long-range force from ~3-6 nm with the experimental decay length λ_{exp} = ~ 1.1 nm. The inset shows the oscillatory region (0-3 nm). (b) Experimental decay length λ_{exp}, plotted as a function of $c^{1/2}$, for NaCl aqueous solutions (red circles), and ionic liquid ([C_4C_1Pyrr][NTf_2]) propylene carbonate solutions (blue symbols), and compared with values in the literature[11] (red diamonds). The solid (ε_r = 80.1) and dashed (ε_r = 64) lines show how the theoretical Debye length varies with $c^{1/2}$ for two values of dielectric constant. Reproduced with permission from Smith *et al*., J. Phys. Chem. Lett. **7**, 2157 (2016). Copyright 2016, American Chemical Society.

IV. Force modulation by surface-attached macromolecules

Polymers on surfaces (whether absorbed or grafted) in a liquid medium are ubiquitous in many different fields including wet adhesion,[224-234] colloidal stability,[235,236] and bio-lubrication.[237-242] The performances of such polymer-bearing surfaces are largely determined by their interfacial interactions, including but not limited to steric interactions (originating in the configurational entropy of the macromolecules), van der Waals forces, electrostatic forces, hydrophobic interactions, hydrogen bonding, hydration forces, π–π stacking, cation–π interactions, and interpenetration and entanglement of polymer chains.[243-245] Recently, using an SFB, a unique anion−π interaction in a marine-bioadhesive-inspired absorbed polymer was identified and evaluated in aqueous solutions.[246] A robust adhesion comparable to the dopa-Fe^{3+} chelation system[247] and cation−π interaction systems[248,249] in this absorbed polymer system consisting of anionic phosphate ester and π-conjugated catecholic moieties (figure 12a) has been reported (figure 12b). The role of the anionic phosphate ester in the robust adhesion was further demonstrated through surface force measurements by varying ions concentration and competition anions (figure 12c). This study exemplifies how the SFB can be exploited to measure specific chemical interactions, in contrast to the more general effects that we have described above.

Polymer brushes, which are polymer chains end-tethered or anchored to a non-adsorbing substrate from which they stretch away in a good solvent, represent an interesting subclass of polymers at surfaces. Such brushes may be either "grafted to" a surface, where end-functionalized chains are added and attach chemically or physically to a surface, or "grafted from" a surface, where they are

polymerized from initiating sites on the surface; each method has its strength and drawbacks. Polymer brushes have found a variety of applications in nanoparticle stabilization (including nanomedicine and pharmaceuticals),[250-253] lubrication,[254-258] and antifouling coatings,[259-261] while the conceptual simplicity of their structure has led to detailed SFB studies of their properties to better understand the physics of such layers.[26,262-265]

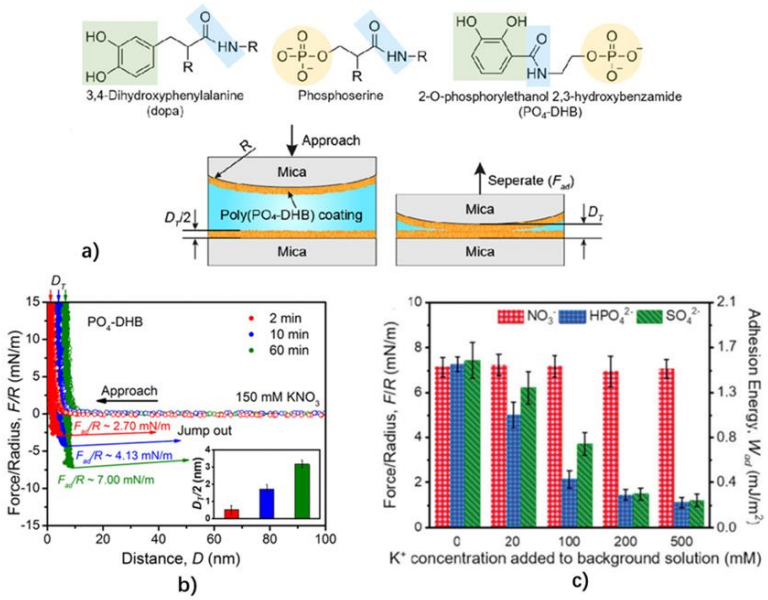

Figure 12. Direct measurement of anion−π interaction in aqueous solution, illustrating how forces arising from chemical interactions may be directly measured. (a) Molecular structures of 3,4-dihydroxyphenethylamine (dopa) and phosphoserine residues, and 2-O-Phosphorylethanol 2,3-hydroxybenzamide (PO_4-DHB). Schematic of SFB measurement of the adhesion force (F_{ad}) between two poly(PO_4-DHB) films. (b) Normalized force versus distance profiles as a function of deposition time t of poly(PO_4-DHB) films in 150 mM KNO_3 solution. The inset shows the thickness of poly(PO_4-DHB) film with different deposition times. (c) Adhesion changes between poly(PO_4-DHB) films after addition of different anions. Reproduced with permission from Zhang *et al.*, J. Am. Chem. Soc. **142**, 1710 (2020). Copyright 2020, American Chemical Society.

Brush-like molecular motifs are also frequently found in biological systems, and a recent SFB study was motivated by the bottlebrush structure of lubricin, a glycoprotein found on articular cartilage surface and in synovial fluid, which plays an important role in cartilage lubrication.[242,266] ABA bottlebrush-like polymers were prepared with two adhesive (A) blocks consisting of positively charged and hydrophobic moieties and a bottlebrush block (B) of the polymer consisting of a flexible backbone decorated with highly hydrated moieties of poly(2-methacryloyloxyethyl phosphorylcholine)] (PMPC) , as shown in figure 13a).[267] This PMPC bottle-brush-like structure resembles PMPC brushes grafted to mica,[264] whose extreme lubricity (friction coefficient $\mu \approx 10^{-4}$) was attributed to hydration lubrication at the highly hydrated phosphocholine monomers. The boundary layers created by ABA polymers, however, while providing good lubrication ($\mu = 0.003$), were less efficient than the model planar brushes[264] by about an order of magnitude, probably as a result of the lower density of the PMPC moieties on the bottlebrush structure. Using the SFB (figure 13b), it was confirmed that the superior antifouling properties (against lysozyme) of the ABA bottlebrush polymers were sustained under high pressure.[172] Such high pressure behaviour seen in the SFB is inaccessible using regular antifouling tests such as surface plasmon resonance (SPR)[268,269] or quartz crystal microbalance with dissipation (QCM-D),[270] which are necessarily carried out under ambient pressure.

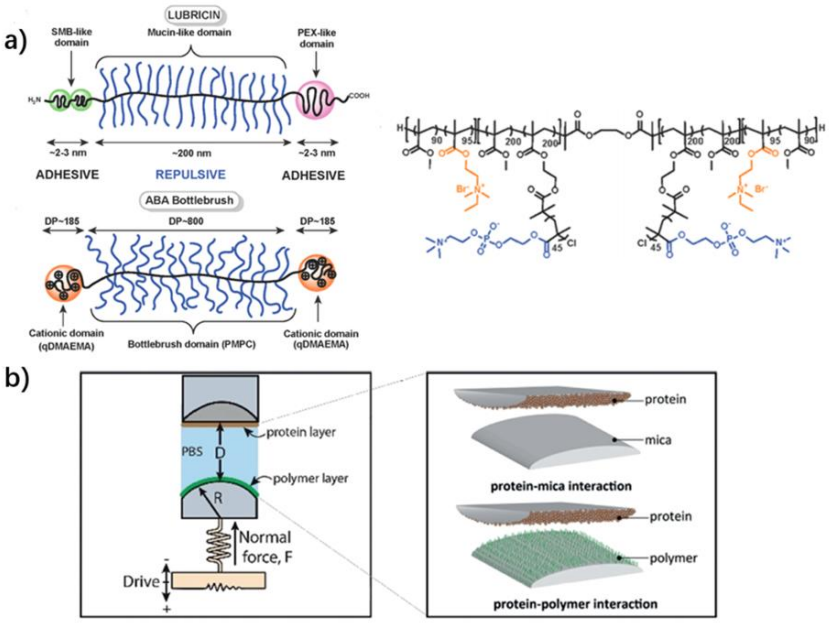

Figure 13. Lubricin-inspired bottlebrushes polymer, and illustration of an SFB protocol for examining its antifouling properties when attached to surfaces. (a) Schematic representations of lubricin and of the ABA bottlebrush polymer mimicking lubricin. (b) Schematic of the SFB setup for the measurements of the interaction between protein (lysozyme)–mica (top) and protein–polymer (bottom). (a) reproduced with permission from Banquy *et al*., J. Am. Chem. Soc. **136**, 6199 (2014). Copyright 2014, American Chemical Society. (b) reproduced with permission from Xia *et al*., Angew. Chem. **58**, 1308 (2019). Copyright 2019, John Wiley and Sons, Inc.

Using the "grafting-from" approach, in a recent SFB study by Tairy *et al*.,[257] PMPC brushes were grown through atom transfer radical polymerization (ATRP) from macroinitiator-coated mica substrates. This study was designed to grow much higher brush densities than previous similar brushes, which leads to much greater high-pressure lubricity compared with earlier studies of PMPC brushes grown from planar (mica) substrates.[264,271] The normal force (F_n/R) vs surface separation D profiles were measured, and well fitted using an expression[272] derived from the Alexander−de Gennes scaling approach,[273]

$$\frac{F_{\mathrm{n}}(D)}{R} = \frac{4\pi kTL}{s^3}\left[\frac{4c_1}{5}\left(\frac{2L}{D}\right)^{5/4} + \frac{4c_2}{7}\left(\frac{D}{2L}\right)^{7/4} - \left(\frac{4c_1}{5} + \frac{4c_2}{7}\right)\right] \qquad (3),$$

where L is the uncompressed brush thickness, s is the mean inter-anchor spacing between brush molecules on the surface, k_B and T are Boltzmann constant and absolute temperature, and c_1, c_2 are undetermined scaling constants of order unity. The density of the polymer brushes may be expressed in terms of the brush thickness to the mean brush spacing ratio (L/s). The ratio (L/s) in Tairy *et al*. study[257] varies from 20 to 50, compared with an (L/s) ≈ 10 in an earlier study[264] on "grafting-from" PMPC brushes, and (L/s) ≈ 8 in the classical SFB study[274] of polystyrene brushes immersed in toluene. Following the Tairy *et al*. study, Iuster *et al*.[275] were able to prepare thin cross-linked PMPC hydrogels and measure the surface interaction between them using an SFB, as in fig. 14. While both brushes and cross-linked brushes exhibit ultralow friction (figure 14a) attributed to hydration lubrication via the highly hydrated phosphocholine groups exposed at the slip plane, there is a marked difference in its dependence on the sliding velocity v_s as shown in figure 14b. This difference is attributed[275] to the self-regulating interpenetration of the opposing chains in the case of the regular brushes, fig. 14(c) top, contrasting with the fixed interpenetration of the cross-linked brushes imposed by the cross-links themselves, fig. 14(c) bottom, recalling that the interpenetration zone is where frictional dissipation occurs.

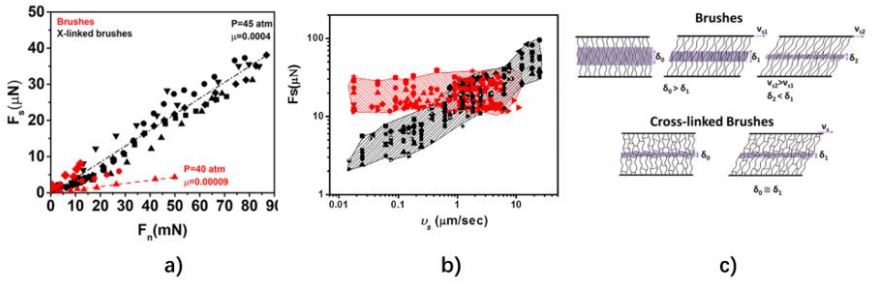

Figure 14. Force measurements illustrating the differing mechanisms of friction between brush-like and the hydrogel-like layers. (a) Comparison of the shear force F_s versus the normal load F_n between PMPC brushes (red symbols) and PMPC cross-linked brushes (black symbols). Shear velocity during these measurements was 1.2−1.5 μm/s. (b) Shear forces F_s versus sliding velocity v_s for PMPC brushes (red symbols) and PMPC cross-linked brushes (black symbols) sliding past each other. (c) Schematic illustrations of interpenetration zone (shaded area) between two compressed layers of either linear brushes or cross-linked brushes. Reproduced with permission from Iuster *et al.*, Macromolecules **50**, 7361 (2017). Copyright 2017, American Chemical Society.

More recently, Yu *et al.*[265] grew dense, charged polystyrene sulfonate brushes from mica surfaces by using a "grafting from" ATRP method, and examined them with an SFB. In low concentration monovalent salt these exhibited low friction ($\mu \approx 10^{-3}$-10^{-4}) up to much higher contact pressures (5 MPa) than a similarly-negatively-charged polymer brush hydrophobically-end attached via a "grafting to" approach, which could maintain low friction only up to 0.3 MPa.[263] This demonstrates the far greater robustness of the grafted from chains. Much higher friction (μ ~ 0.15-0.3) was measured with these charged brushes in the presence of tiny concentrations of multivalent ions, and attributed to bridging and to brush collapse.[265] It is of interest that "grafted-to" zwitterionic PMPC bottle-brushes are significantly more lubricious at such low concentrations of multivalent ions than the "grafted-from" polyelectrolyte brushes ("grafting-from" method), suggesting much weaker multivalent ion/zwitterion interactions.[276]

V. The versatility of amphiphiles

Amphiphiles are molecules with both hydrophobic and hydrophilic moieties (such as surfactants, phospholipids, or amphiphilic polymers). Such molecules, through a combination of entropic and enthalpic factors, often self-assemble into aggregates of various shapes and sizes. These include micelles, vesicles, lamellae, nanofibers, and nanotubes in aqueous solution or at interfaces,[277,278] and are widely used in diverse fields from drug delivery to cosmetic formulations. Understanding such structures at interfaces has long attracted both theoretical and experimental attention,[279,280] not least studies of the forces between surfaces bearing amphiphilic assemblies, which, together with microscopic imaging of their structure, shed strong light on their interfacial properties.

5.1 Surfactants

When negatively charged surfaces interact across bulk aqueous solutions of cationic or zwitterionic surfactants (above their critical micellization concentration), they are often coated by a homogenous layer of wormlike micelles or hemi-micelles.[281,282] Using an SFB, the frictional energy dissipation between two such surfaces sliding past each other was observed to be very low (with a friction coefficient $\mu \sim 10^{-3}$-10^{-4}).[283-285] This was attributed to hydration lubrication at the slip-plane between the exposed, hydrated charged or zwitterionic headgroups. This lubricity breaks down at sufficiently high compressions when the absorbed micellar layers hemi-fuse into a bilayer between the surfaces. This transition is modulated by the chain length of the surfactant molecules, surface charge density on the adsorbing surface, and types of counterion, while the collapse from bilayer or micellar structure to a monolayer can be directly seen in the SFB by monitoring the surface separation D directly (at sub-nanometer resolution) at the same time as the increase in friction.[192,284]

Hydrophobic interactions are ubiquitous both in technology and in biology, where they play a major role in the structure of biomacromolecules, and the forces across water between hydrophobized surfaces have long been studied in the SFB. Hydrophobic surfactant monolayers on mica can be formed either by Langmuir-Blodgett deposition from an aqueous sub-phase[286,287] or by self-assembly from solution into a bilayer which loses its top layer on withdrawal through the liquid-air interface;[288,289] in both cases a uniform layer of hydrophobic tails is exposed. Direct studies of the forces between such surfaces revealed long-ranged so-called hydrophobic attractions – at surface separations up to order 100 nm or more – whose origins were a puzzle for many years.[10] A deep insight into the nature of these forces emerged in recent years from SFB studies carried out by a number of groups.[288-296] While such surfaces in air were uniform and highly hydrophobic, as revealed by water droplet contact angles, it was found by AFM imaging that rearrangement with time under water of the initially uniform surfactant monolayer resulted in their break-up into heterogeneous surfaces coated by random positive and negative charge domains. The long-ranged attraction between such overall-neutral surfaces across water was then attributed, by several groups independently[290-293,295] to the presumed movement of such domains so that positive domains on one surface faced negative domains on the other, resulting in a long-ranged electrostatic attraction. Subsequently Silbert *et al*.[289] showed that there was no need to assume any correlation between opposing, oppositely-charged domains. Using the SFB in a combined normal and lateral motion mode, it was demonstrated that even a random, overall-neutral, quenched charge domain array facing a similar random array would experience an overall long-ranged attraction of electrostatic origin (rather than any hydrophobic effect). The attraction arises because of the qualitatively

different mechanisms of repulsion and attraction across water between equally-charged and between oppositely-charged surfaces, respectively, as shown in figure 15.

The former may be viewed as due to the osmotic pressure of trapped counterions at the midplane, while the latter may be seen as arising from the entropy gain upon release of counterion pairs from within the gap between the approaching surfaces. In other words, two oppositely charged surfaces across water attract more than two similarly charged ones repel, for the same interacting areas, absolute surface charge densities and surface separations, and a simple model indeed shows good agreement with the experimental data[289] (figure 15 broken red curve). These conclusions were later supported by more detailed theoretical calculations.[297,298] The deep insight from these experiments is that, what was for decades regarded as a long-ranged 'hydrophobic attraction' between overall-neutral surfactant-hydrophobized surfaces – the bulk of experiments on the hydrophobic interaction[10,286,287,299]– could be understood rather as a long-ranged electrostatic attraction between random charge patches or grain boundaries.

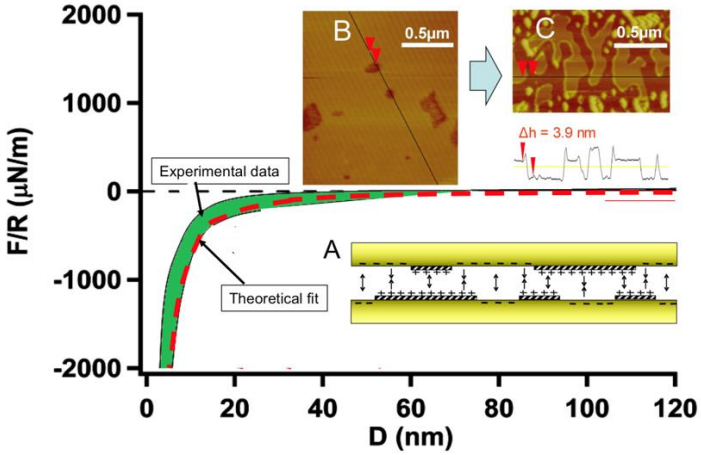

Figure 15. Illustrating the origins of the long-ranged attraction between hydrophobized surfaces by surfactant layers. Main figure: Showing the SFB experimentally-measured attraction (green curve) and the theoretically calculated one (red broken curve) evaluated by numerical solution of the integrated Poisson-Boltzmann equation for interactions between two overall-neutral surfaces coated with patches of positive and negative charges (schematic in inset A), as revealed for surfaces hydrophobized with C_{18}TAB surfactant after immersion in water. Inset B: A mica surface that had been hydrophobized with C_{16}TAB, imaged with AFM 5 min after coverage by water; the surface is mostly molecularly smooth. Inset C: as inset B, but following 30 mins coverage by water, showing clear break-up of the originally-smooth surface into bilayer patches. Reproduced with permission from Klein. Adv. Colloid Interface Sci. **270**, 261 (2019). Copyright 2019, Elsevier.

5.2 Phospholipids

Phosphatidylcholine (PC) lipids are a major class of phospholipids, which consist of one hydrophilic phosphocholine headgroup and two hydrophobic fatty acid tails. In aqueous solutions, they may self-assemble into lipid bilayers, micelles, or liposomes. The highly hydrated nature of the phosphocholine groups (each phosphocholine group binds 15 or more water molecules in the primary hydration layer[300-303]) was earlier shown to lead to extreme reduction in friction between phosphocholinated polymer brushes;[264,271] using an SFB, Goldberg *et al*.[304] extended this to examine PC liposomes exposing their phosphocholine groups in 2-D arrays. Close-packed layers of

hydrogenated soy phosphatidylcholine (HSPC) liposomes were deposited on mica surfaces and the friction coefficients between these layers was as low as 10^{-4}-10^{-5} in water and 10^{-3}-10^{-4} at physiologically high salt concentration,[304,305] up to pressures comparable to that in the major joints (hips or knees, where local contact stresses can reach 10 MPa or more). This large reduction in frictional dissipation was attributed to hydration lubrication by the close-packed, highly hydrated phosphocholine groups. Subsequently, Sorkin *et al*.[35] showed that the lubrication performance of lipid boundary layers across lipid-free water was correlated with their robustness, with gel-phase bilayers lubricating to higher pressures than liquid phase lipids. Interestingly, this trend is reversed when the measurements are carried out in dispersions of the liposomes,[306] an unexpected result attributed to rapid self-healing of the liquid-phase bilayers, enabled by available lipids in the surrounding medium, together with the higher hydration level of their headgroups.

The strong lubricity afforded by boundary layers of lipid vesicles raises the question of their stability with time against aggregation when in dispersion prior to being introduced to surfaces. This is essential for any practical application, whether the liposomes are in the form of small unilamellar or larger multilamellar vesicles (SUVs or MLVs). The gold-standard approach for the stabilization of vesicles is by incorporating PEGylated lipids (poly(ethylene glycol), PEG) into the lipid bilayer (so-called PEGylation[307,308]); such chains stretch away from the surface, providing a steric barrier suppressing vesicle aggregation. However, PEGylation may also weaken the lubrication ability of the PC vesicles, due to the PEG corona which is considerably less hydrated than the phosphocholine headgroups.[304] By substituting the weak hydration of PEG by highly-hydrated moieties of PMPC, Lin *et al*.[251] made PMPCylated liposomes that exhibit an excellent colloidal stability in water or

physiological saline solution, while providing a lubricity fully equal to that of bare liposomes (recalling however that the latter are not stable), and which are ten times more lubricious than PEGylated liposomes. Such stabilized liposomes would have wide practical applications, for instance, for delivery with a designed lubrication and thereby alleviation of widespread pathologies loss of lubricity such as osteoarthritis, tendonitis, or dry eye syndrome.[309,310]

These SFB results have clear implications for biolubrication phenomena, since PC lipids (and other lipids with hydrated headgroups) are ubiquitous in the body.[311,312] Recent SFB investigations by Seror *et al*. and Zhu *et al*.[169,313] led to a new model proposed for how PC lipids may form highly lubricous layers on the outermost surface of articular cartilage in the synovial joint. In these studies, hyaluronic acid（HA) molecules were attached to the substrate surface via avidin-biotin linkage, to resemble their presence at the articular cartilage surface. The introduction of PC lipids was in the formation of SUVs. These lipids (either HSPC or DPPC, dipalmitoylphosphatidylcholine, both in their gel-state during the experiments at room temperature) complexed with the surface-linked HA, and were found to maintain as low friction as $\mu \sim 0.001$ up to the highest contact stresses related to major joints such as knees and hips (up to order 10 MPa), through the hydration lubrication mechanism. For the lipids (DMPC, dipalmitoylphosphatidylcholine and POPC, 1-palmitoyl-2-oleoyl-sn-glycero-3-phosphocholine) in fluid state, the complexes (HA-DMPC and HA-POPC) sustained reduction in friction only at lower pressure (less than 2 MPa) due to the weaker van der Waals forces between the hydrocarbon tails,[169] whereas the even more fluid lipid (DOPC, 1,2-dioleoyl-sn-glycero-3-phosphocholine) didn't enhance the lubrication of HA layers, possibly because of the limited robustness of such layers (well above their gel-to-liquid-phase transition

tempeartiure) to mechanical stresses.[24] Synovial joints and fluids contain many different types of lipids, and more recently Cao *et al*.[314,315] investigated the lubrication performance using mixture lipids (binary lipids and extracted lipids from synovial fluid). These studies prove that SFB can be used for more complex multilayers and physiologically relevant environments, and demonstrate well how the direct force measurement studies can lead to new insights into macroscopic biological mechanisms.[316] Indeed, there is some evidence that multicomponent lipid mixtures with components similar to those found in synovial joints can provide a synergistic effect in boundary lubrication.[317]

In other lipid related studies, the different effects of glycerol and dimethyl sulfoxide (DMSO) (widely used penetrating cryoprotective agents) on the surface hydration of a DPPC bilayer were investigated, as these molecules are known to compete for the hydration water surrounding the lipid headgroups.[318,319] At low concentration of DMSO (0-10 mol%), DMSO decreases the hydration shell of the phosphocholine headgroup, and therefore induces a shorter-ranged repulsive interaction, while at higher concentration of DMSO（10-20 mol%), DMSO inhibits the PC headgroups random thermal motion by dehydrating the headgroup and collapsing them down to the bilayer surface. On the other hand, glycerol has some similarity with water structure at the molecular level, which interacts with lipid headgroup similarly to water and induces a longer-ranged repulsion.[318,319] For more specific studies of bilayers, a fluorescence SFB was developed and used to determine the force profiles and image the real-time hemifusion process between bilayers composed of phase-separated domains in the contact area simultaneously.[320] Results show lipid-disordered and lipid-ordered domains, and reveal clearly the dynamic transformation during hemifusion. The use of fluorescence SFB may enable extension of the previous study[36] of the selective adsorption of myelin basic protein

(MBP) on the lipid-disordered domain, to monitor dynamic MBP adsorption under different lipid phase-states upon heating or cooling the system.

5.3 Amphiphilic polymers

In order to address the problems of instability and more complicated preparation of liposomes, while at the same time retaining their lubricity arising from the strong phosphocholine hydration, amphiphilic polymers including homo-oligomeric molecules and poly-phosphorylcholine block copolymers were created.[284] Compared with the poor lubricity of block copolymer and the pressure intolerance of single-chain surfactant micelles,[193,321] the oligomeric phosphorylcholine micelle formed a tenacious boundary layer under pressure and shear, with excellent lubrication performance and structural stability. The highly-hydrated phosphocholine (phosphorylcholine) groups ensure hydration lubrication by the micelles, while the polymerization of the hydrophobic part enhances the interaction of the hydrophobic region, thereby enhancing its compressive performance. Boundary layers of the oligomeric phosphocholine micelles exhibit low friction coefficients (~ 0.004) up to high compressions (> 5 MPa), thereby extending liposome lubricants to highly-stable micellar lubricants that are easy to prepare. Other lubricating nanoparticles (NPs) have also been studied in the SFB. An attempt to modify polystyrene NPs by phosphocholine surface moieties[322] revealed that they formed a single bridging layer between mica surfaces, and so did not provide the hoped for reduction in frictional dissipation on sliding. However, NPs of phytoglycogen, a single-molecule highly branched polysaccharide, exhibit excellent water retention, due to the abundance of close-packed hydroxyl groups forming hydrogen bonds with water. Such phytoglycogen NPs

thus constituted good lubricants – via the hydration lubrication mechanism - when attached at surfaces, as revealed by a very recent SFB study.[323]

VI. Conclusions and challenges

Direct force measurements between model surfaces using the mica surface forces balance, SFB (or surface force apparatus, SFA), have resulted in major new insights and applications since the early first experiments in the late 1960's. We have reviewed recent progress, largely over the past decade or so, focusing on different aspects. These include new measurement configurations, the extension of the traditionally-used mica substrates to other surfaces enabling, *inter alia*, controlled surface potentials, and new insights into the behaviour of a large range of confined simple and structured fluids. It is notable that the microscopic SFB studies down to nanometer, and sometimes sub-nanometer surface separations, may have direct implications for novel macroscopic applications. These include the discovery of hydration lubrication leading to the use of liposomes in potential dry-eye and osteoarthritis treatments;[324] in the creation of highly-lubricated hydrogels;[185] or the identification of novel molecules such as highly-hydrated, biomimicking bottle-brush molecules,[325] or ionic liquids,[326] to serve as environmentally-friendly lubricants.

Finally, we may identify new challenges and opportunities related to direct force measurements with the SFB. These include:

1) Exploiting fast or ultra-fast video recordings of the motion and shape of interference fringes (FECO) during dynamic surface forces measurements, to reveal behaviour at short times of highly

confined liquids in different configurations (including under high electric fields, or cavitation between hydrophobic surfaces)

2) Extending direct force measurements between more biologically-relevant surface structures, providing insight into interactions in living systems.

3) Utilizing the increasingly higher power of computers and novel computational approaches to carry out more realistic (e.g. all-atom) simulations of interactions between surfaces across both simple liquids and more complicated molecular systems (e.g. lipids or polymers) both to understand effects at the molecular level, and to inform design of future experiments.

4) Incorporation of other techniques, such as fluorescence microscopy or infrared spectroscopy, which allows for getting more information other than force signals during measurements. For example, combined with a fluorescence microscope, it might be able to track the two-dimensional morphology of the lubricating boundary layer, the distribution of specific molecules in the lubricating layer, and possible wear conditions during the friction process in real-time (as already indicated in one recent study). Combining SFB measurements with direct imaging of the surfaces *at the actual area of contact* (identified possibly fluorescently), using e.g. scanning probe (AFM) or electron microscopy methods, would provide more direct insight into the nature of interaction and wear, especially where boundary layers on the mica are present.

Acknowledgements

The authors thank the McCutchen Foundation, the Rothschild Caesarea Foundation, the Israel Ministry of Science and Industry (grant 713272), the Israel Science Foundation (grant 1229/20) and the Israel Science Foundation-National Science Foundation China joint program (grant ISF-NSFC

2577/17) for support of some of the work described in this review. This project has received funding from the European Research Council (ERC) under the European Union's Horizon 2020 research and innovation program (grant No. 743016). This work was made possible in part by the historic generosity of the Harold Perlman family.

Data availability

Data sharing is not applicable to this review as no new data were created or analyzed within the article.

References

1 Tabor, D. & Winterton, R. Surface forces: Direct measurement of normal and retarded van der Waals forces. *Nature* **219**, 1120-1121 (1968).

2 Israelachvili, J. N. & Tabor, D. Measurement of van der Waals dispersion forces in the range 1.4 to 130 nm. *Nature* **236**, 106-106 (1972).

3 J. N. Israelachvili & Adams, G. E. Direct measurement of long range forces between two mica surfaces in aqueous KNO3 solutions. *Nature* **262**, 774-776 (1976).

4 Israelachvili, J. N. & Adams, G. E. Measurement of forces between two mica surfaces in aqueous electrolyte solutions in the range 0–100 nm. *J. Chem. Soc., Faraday Trans. 1* **74**, 975-1001 (1978).

5 Horn, R. G. & Israelachvili, J. N. Direct measurement of structural forces between two surfaces in a nonpolar liquid. *J. Chem. Phys.* **75**, 1400-1411 (1981).

6 Klein, J. Forces between mica surfaces bearing layers of adsorbed polystyrene in cyclohexane. *Nature* **288**, 248-250 (1980).

7 Klein, J. Forces between mica surfaces bearing adsorbed macromolecules in liquid media. *J. Chem. Soc., Faraday Trans. 1* **79**, 99-118 (1983).

8 Christenson, H. K., Horn, R. G. & Israelachvili, J. N. Measurement of forces due to structure in hydrocarbon liquids. *J. Colloid Interface Sci.* **88**, 79-88 (1982).

9 Israelachvili, J. N. & Pashley, R. M. The hydrophobic interaction is long range, decaying exponentially with distance. *Nature* **300**, 341-342 (1982).

10 Christenson, H. K. & Claesson, P. M. Direct measurements of the force between hydrophobic surfaces in water. *Adv. Colloid Interface Sci.* **91**, 391-436 (2001).

11 Pashley, R. M. DLVO and hydration forces between mica surfaces in Li+, Na+, K+, and Cs+ electrolyte solutions: A correlation of double-layer and hydration forces with surface cation exchange properties. *J. Colloid Interface Sci.* **83**, 531-546 (1981).

12 Pashley, R. M. & Israelachvili, J. N. DLVO and hydration forces between mica surfaces in Mg2+, Ca2+, Sr2+, and Ba2+ chloride solutions. *J. Colloid Interface Sci.* **97**, 446-455 (1984).

13 Pashley, R. M. Hydration forces between mica surfaces in aqueous electrolyte solutions. *J. Colloid Interface Sci.* **80**, 153-162 (1981).

14 Israelachvili, J. N. & Pashley, R. M. Molecular layering of water at surfaces and origin of repulsive hydration forces. *Nature* **306**, 249-250 (1983).

15 Raviv, U. & Klein, J. Fluidity of Bound Hydration Layers. *Science* **297**, 1540-1543, doi:10.1126/science.1074481 (2002).

16 Klein, J., Perahia, D. & Warburg, S. Forces between polymer-bearing surfaces undergoing shear. *Nature* **352**, 143-145 (1991).

17 Leckband, D. The surface apparatus--a tool for probing molecular protein interactions. *Nature* **376**, 617-618 (1995).

18 Wong, J. Y., Kuhl, T. L., Israelachvili, J. N., Mullah, N. & Zalipsky, S. Direct measurement of a tethered ligand-receptor interaction potential. *Science* **275**, 820-822 (1997).

19 Israelachvili, J. N. & Tabor, D. The shear properties of molecular films. *Wear* **24**, 386-390 (1973).

20 Yoshizawa, H., Chen, Y. L. & Israelachvili, J. Fundamental mechanisms of interfacial friction. 1. Relation between adhesion and friction. *J. Phys. Chem.* **97**, 4128-4140 (1993).

21 Yoshizawa, H. & Israelachvili, J. Fundamental mechanisms of interfacial friction. 2. Stick-slip

friction of spherical and chain molecules. *J. Phys. Chem.* **97**, 11300-11313 (1993).

22 Bhushan, B., Israelachvili, J. N. & Landman, U. Nanotribology: friction, wear and lubrication at the atomic scale. *Nature* **374**, 607-616 (1995).

23 Zeng, H., Maeda, N., Chen, N., Tirrell, M. & Israelachvili, J. Adhesion and friction of polystyrene surfaces around T g. *Macromolecules* **39**, 2350-2363 (2006).

24 Yu, J., Banquy, X., Greene, G. W., Lowrey, D. D. & Israelachvili, J. N. The boundary lubrication of chemically grafted and cross-linked hyaluronic acid in phosphate buffered saline and lipid solutions measured by the surface forces apparatus. *Langmuir* **28**, 2244-2250 (2012).

25 Yu, J. *et al.* Friction and adhesion of gecko-inspired PDMS flaps on rough surfaces. *Langmuir* **28**, 11527-11534 (2012).

26 Klein, J., Kumacheva, E., Mahalu, D., Perahia, D. & Fetters, L. J. Reduction of frictional forces between solid surfaces bearing polymer brushes. *Nature* **370**, 634-636 (1994).

27 Kumacheva, E. & Klein, J. Simple liquids confined to molecularly thin layers. II. Shear and frictional behavior of solidified films. *J. Chem. Phys.* **108**, 7010-7022, doi:10.1063/1.476115 (1998).

28 Craig, V. S. An historical review of surface force measurement techniques. *Colloids Surf. A Physicochem. Eng.* **129**, 75-93 (1997).

29 Kurihara, K. Surface forces measurement for materials science. *Pure Appl. Chem.* **91**, 707-716, doi:10.1515/pac-2019-0101 (2019).

30 Cheng, H.-W. & Valtiner, M. Forces, structures, and ion mobility in nanometer-to-subnanometer extreme spatial confinements: Electrochemisty and ionic liquids. *Curr. Opin. Colloid Interface Sci.* **47**, 126-136, doi:10.1016/j.cocis.2020.02.003 (2020).

31 Xiang, L., Zhang, J., Gong, L. & Zeng, H. Surface forces and interaction mechanisms of soft thin films under confinement: a short review. *Soft Matter* **16**, 6697-6719, doi:10.1039/d0sm00924e (2020).

32 Butt, H.-J. Measuring electrostatic, van der Waals, and hydration forces in electrolyte solutions with an atomic force microscope. *Biophys. J.* **60**, 1438-1444 (1991).

33 Ducker, W. A., Senden, T. J. & Pashley, R. M. Direct measurement of colloidal forces using an atomic force microscope. *Nature* **353**, 239-241 (1991).

34 Perkin, S. *et al.* Forces between Mica Surfaces, Prepared in Different Ways, Across Aqueous and Nonaqueous Liquids Confined to Molecularly Thin Films. *Langmuir* **22**, 6142-6152, doi:10.1021/la053097h (2006).

35 Sorkin, R., Kampf, N., Dror, Y., Shimoni, E. & Klein, J. Origins of extreme boundary lubrication by phosphatidylcholine liposomes. *Biomaterials* **34**, 5465-5475, doi:10.1016/j.biomaterials.2013.03.098 (2013).

36 Lee, D. W. *et al.* Lipid domains control myelin basic protein adsorption and membrane interactions between model myelin lipid bilayers. *Proc. Natl. Acad. Sci. U. S. A.* **111**, E768-E775, doi:10.1073/pnas.1401165111 (2014).

37 Pick, C., Argento, C., Drazer, G. & Frechette, J. Micropatterned charge heterogeneities via vapor deposition of aminosilanes. *Langmuir* **31**, 10725-10733, doi:10.1021/acs.langmuir.5b02771 (2015).

38 Giraud, L., Bazin, G. & Giasson, S. Lubrication with Soft and Hard Two-Dimensional Colloidal Arrays. *Langmuir* **33**, 3610-3623, doi:10.1021/acs.langmuir.7b00006 (2017).

39 Kurniawan, J., Suga, K. & Kuhl, T. L. Interaction forces and membrane charge tunability: Oleic

acid containing membranes in different pH conditions. *Biochim Biophys Acta Biomembr.* **1859**, 211-217 (2017).

40 Dziadkowiec, J., Javadi, S., Bratvold, J. E., Nilsen, O. & Royne, A. Surface Forces Apparatus Measurements of Interactions between Rough and Reactive Calcite Surfaces. *Langmuir* **34**, 7248-7263, doi:10.1021/acs.langmuir.8b00797 (2018).

41 Huang, J. *et al.* Probing the Self-Assembly and Nonlinear Friction Behavior of Confined Gold Nano-Particles. *Langmuir* **35**, 15701-15709, doi:10.1021/acs.langmuir.9b02172 (2019).

42 Redeker, C. & Briscoe, W. H. Interactions between Mutant Bacterial Lipopolysaccharide (LPS-Ra) Surface Layers: Surface Vesicles, Membrane Fusion, and Effect of Ca(2+)and Temperature. *Langmuir* **35**, 15739-15750, doi:10.1021/acs.langmuir.9b02609 (2019).

43 Wang, J. *et al.* Molecular Interactions of a Polyaromatic Surfactant C5Pe in Aqueous Solutions Studied by a Surface Forces Apparatus. *J. Phys. Chem. B* **116**, 11187-11196, doi:10.1021/jp304444d (2012).

44 Ajiro, H. *et al.* Force Estimation on the Contact of Poly(l,l-lactide) and Poly(d,d-lactide) Surfaces Regarding Stereocomplex Formation. *Langmuir* **32**, 9501-9506, doi:10.1021/acs.langmuir.6b02623 (2016).

45 Kan, Y. J., Yang, L., Tan, Y., Wei, Z. Y. & Chen, Y. F. Diminishing Cohesion of Chitosan Films in Acidic Solution by Multivalent Metal Cations. *Langmuir* **36**, 4964-4974, doi:10.1021/acs.langmuir.0c00438 (2020).

46 Vialar, P., Merzeau, P., Giasson, S. & Drummond, C. Compliant Surfaces under Shear: Elastohydrodynamic Lift Force. *Langmuir* **35**, 15605-15613, doi:10.1021/acs.langmuir.9b02019 (2019).

47 de Aguiar, H. B., McGraw, J. D. & Donaldson, S. H. Interface-Sensitive Raman Microspectroscopy of Water via Confinement with a Multimodal Miniature Surface Forces Apparatus. *Langmuir* **35**, 15543-15551, doi:10.1021/acs.langmuir.9b01889 (2019).

48 Israelachvili., J. N. *et al.* Recent advances in the surface forces apparatus (SFA) technique. *Rep. Prog. Phys.* **73**, 036601, doi:10.1088/0034-4885/73/3/036601 (2010).

49 Christenson, H. K. & Thomson, N. H. The nature of the air-cleaved mica surface. *Surf. Sci. Rep.* **71**, 367-390 (2016).

50 Israelachvili, J. N. *et al.* The Intersection of Interfacial Forces and Electrochemical Reactions. *J. Phys. Chem. B* **117**, 16369-16387, doi:10.1021/jp408144g (2013).

51 Kasuya, M. *et al.* Characterization of Water Confined between Silica Surfaces Using the Resonance Shear Measurement. *J. Phys. Chem. C* **117**, 13540-13546, doi:10.1021/jp404378b (2013).

52 Tivony, R. & Klein, J. Probing the Surface Properties of Gold at Low Electrolyte Concentration. *Langmuir* **32**, 7346-7355, doi:10.1021/acs.langmuir.6b01697 (2016).

53 Balabajew, M., Van Engers, C. D. & Perkin, S. Contact-free calibration of an asymmetric multi-layer interferometer for the surface force balance. *Rev. Sci. Instrum.* **88**, 123903 (2017).

54 Han, M. W. & Espinosa-Marzal, R. M. Electroviscous Retardation of the Squeeze Out of Nanoconfined Ionic Liquids. *J. Phys. Chem. C* **122**, 21344-21355, doi:10.1021/acs.jpcc.8b04778 (2018).

55 Dobbs, H. A. *et al.* Electrochemically Enhanced Dissolution of Silica and Alumina in Alkaline Environments. *Langmuir* **35**, 15651-15660, doi:10.1021/acs.langmuir.9b02043 (2019).

56 Richter, L. *et al.* Ions in an AC Electric Field: Strong Long-Range Repulsion between Oppositely

Charged Surfaces. *Phys. Rev. Lett.* **125**, 056001, doi:10.1103/PhysRevLett.125.056001 (2020).

57 Knarr, R. F., Quon, R. A. & Vanderlick, T. K. Direct force measurements at the smooth gold/mica interface. *Langmuir* **14**, 6414-6418 (1998).

58 Chai, L. & Klein, J. Large area, molecularly smooth (0.2 nm rms) gold films for surface forces and other studies. *Langmuir* **23**, 7777 See also Research Highlight in Nature 7447 (2007) 7889. (2007).

59 Chai, L. *Forces between polymer-and charge-bearing surfaces across aqueous media* Ph.D. Thesis. section III.2.2 Weizmann Institute thesis, (2007).

60 Chai, L. & Klein, J. Interactions between molecularly smooth gold and mica surfaces across aqueous solutions. *Langmuir* **25**, 11533-11540, doi:10.1021/la9014527 (2009).

61 Gebbie, M. A. *et al.* Ionic liquids behave as dilute electrolyte solutions. *Proc. Natl. Acad. Sci.* **110**, 9674-9679 (2013).

62 Levine, Z. A. *et al.* Surface force measurements and simulations of mussel-derived peptide adhesives on wet organic surfaces. *Proc. Natl. Acad. Sci.* **113**, 4332-4337 (2016).

63 Fujii, S., Kasuya, M. & Kurihara, K. Characterization of Platinum Electrode Surfaces by Electrochemical Surface Forces Measurement. *J. Phys. Chem. C* **121**, 26406-26413, doi:10.1021/acs.jpcc.7b09301 (2017).

64 Shrestha, B. R., Baimpos, T., Raman, S. & Valtiner, M. Angstrom-Resolved Real-Time Dissection of Electrochemically Active Noble Metal Interfaces. *ACS Nano* **8**, 5979-5987, doi:10.1021/nn501127n (2014).

65 Yang, Y., Singh, J. & Ruths, M. Friction of aromatic thiol monolayers on silver: SFA and AFM studies of adhesive and non-adhesive contacts. *RSC Adv.* **4**, 18801-18810, doi:10.1039/c4ra01803f (2014).

66 Shrestha, B. R. *et al.* Real-Time Monitoring of Aluminum Crevice Corrosion and Its Inhibition by Vanadates with Multiple Beam Interferometry in a Surface Forces Apparatus. *J. Electrochem. Soc.* **162**, C327-C332, doi:10.1149/2.0501507jes (2015).

67 Kasuya, M. *et al.* Nanotribological Characterization of Lubricants between Smooth Iron Surfaces. *Langmuir* **33**, 3941-3948, doi:10.1021/acs.langmuir.7b00148 (2017).

68 Valtiner, M., Kristiansen, K., Greene, G. W. & Israelachvili, J. N. Effect of surface roughness and electrostatic surface potentials on forces between dissimilar surfaces in aqueous solution. *Adv. Mater.* **23**, 2294-2299, doi:10.1002/adma.201003709 (2011).

69 Valtiner, M., Banquy, X., Kristiansen, K., Greene, G. W. & Israelachvili, J. N. The Electrochemical Surface Forces Apparatus: The Effect of Surface Roughness, Electrostatic Surface Potentials, and Anodic Oxide Growth on Interaction Forces, and Friction between Dissimilar Surfaces in Aqueous Solutions. *Langmuir* **28**, 13080-13093, doi:10.1021/la3018216 (2012).

70 Tivony, R., Yaakov, D. B., Silbert, G. & Klein, J. Direct Observation of Confinement-Induced Charge Inversion at a Metal Surface. *Langmuir* **31**, 12845-12849, doi:10.1021/acs.langmuir.5b03326 (2015).

71 Tivony, R., Safran, S., Pincus, P., Silbert, G. & Klein, J. Charging dynamics of an individual nanopore. *Nat. Commun.* **9**, 4203, doi:10.1038/s41467-018-06364-1 (2018).

72 Merlet, C. *et al.* On the molecular origin of supercapacitance in nanoporous carbon electrodes. *Nat. Mater.* **11**, 306-310 (2012).

73 Chabi, S., Peng, C., Hu, D. & Zhu, Y. Ideal three‐dimensional electrode structures for electrochemical energy storage. *Adv. Mater.* **26**, 2440-2445 (2014).

74 Breitsprecher, K., Holm, C. & Kondrat, S. Charge me slowly, I am in a hurry: Optimizing charge–discharge cycles in nanoporous supercapacitors. *ACS Nano* **12**, 9733-9741 (2018).

75 Donaldson, S. H. *et al.* Electrochemical control of specific adhesion between amine-functionalized polymers and noble metal electrode interfaces. *Mater. Corros.* **65**, 362-369, doi:10.1002/maco.201307581 (2014).

76 Moeremans, B. *et al.* Lithium-ion battery electrolyte mobility at nano-confined graphene interfaces. *Nat. Commun.* **7**, 1-7 (2016).

77 Merola, C. *et al.* In situ nano- to microscopic imaging and growth mechanism of electrochemical dissolution (e.g., corrosion) of a confined metal surface. *Proc. Natl. Acad. Sci.* **114**, 9541-9546, doi:10.1073/pnas.1708205114 (2017).

78 Moeremans, B. *et al.* In Situ Mechanical Analysis of the Nanoscopic Solid Electrolyte Interphase on Anodes of Li-Ion Batteries. *Adv. Sci.* **6**, doi:10.1002/advs.201900190 (2019).

79 De Levie, R. On porous electrodes in electrolyte solutions: I. Capacitance effects. *Electrochim. Acta* **8**, 751-780 (1963).

80 Biesheuvel, P. & Bazant, M. Nonlinear dynamics of capacitive charging and desalination by porous electrodes. *Phys. Rev. E* **81**, 031502 (2010).

81 Mirzadeh, M., Gibou, F. & Squires, T. M. Enhanced charging kinetics of porous electrodes: Surface conduction as a short-circuit mechanism. *Phys. Rev. Lett.* **113**, 097701 (2014).

82 Zhu, Y. *et al.* Graphene and graphene oxide: synthesis, properties, and applications. *Adv. Mater.* **22**, 3906-3924 (2010).

83 Bitounis, D., Ali‐Boucetta, H., Hong, B. H., Min, D. H. & Kostarelos, K. Prospects and challenges of graphene in biomedical applications. *Adv. Mater.* **25**, 2258-2268 (2013).

84 Huang, L., Zhang, M., Li, C. & Shi, G. Graphene-based membranes for molecular separation. *J. Phys. Chem. Lett.* **6**, 2806-2815 (2015).

85 Britton, J. *et al.* A graphene surface force balance. *Langmuir* **30**, 11485-11492 (2014).

86 Huo, C., Yan, Z., Song, X. & Zeng, H. 2D materials via liquid exfoliation: a review on fabrication and applications. *Sci. Bull.* **60**, 1994-2008 (2015).

87 Liu, X. & Hersam, M. C. Interface characterization and control of 2D materials and heterostructures. *Adv. Mater.* **30**, 1801586 (2018).

88 van Engers, C. D. *et al.* Direct measurement of the surface energy of graphene. *Nano Lett.* **17**, 3815-3821 (2017).

89 Johnson, K. L., Kendall, K. & Roberts, A. Surface energy and the contact of elastic solids. *Proc. Math. Phys. Eng. Sci.* **324**, 301-313 (1971).

90 Cao, Y. *et al.* Correlated insulator behaviour at half-filling in magic-angle graphene superlattices. *Nature* **556**, 80-84 (2018).

91 Cao, Y. *et al.* Unconventional superconductivity in magic-angle graphene superlattices. *Nature* **556**, 43-50 (2018).

92 Dayo, A., Alnasrallah, W. & Krim, J. Superconductivity-dependent sliding friction. *Phys. Rev. Lett.* **80**, 1690 (1998).

93 Park, J. Y., Ogletree, D., Thiel, P. & Salmeron, M. Electronic control of friction in silicon pn junctions. *Science* **313**, 186-186 (2006).

94 Van Engers, C., Balabajew, M., Southam, A. & Perkin, S. A 3-mirror surface force balance for the investigation of fluids confined to nanoscale films between two ultra-smooth polarizable electrodes. *Rev. Sci. Instrum.* **89**, 123901 (2018).

95 Kasuya, M. & Kurihara, K. Novel Surface Forces Apparatus for Characterizing Solid-Liquid Interfaces. *Electrochemistry* **82**, 317-321, doi:10.5796/electrochemistry.82.317 (2014).

96 Kamijo, T., Kasuya, M., Mizukami, M. & Kurihara, K. Direct Observation of Double Layer Interactions between the Potential-controlled Gold Electrode Surfaces Using the Electrochemical Surface Forces Apparatus. *Chem. Lett.* **40**, 674-675, doi:10.1246/cl.2011.674 (2011).

97 Kasuya, M. & Kurihara, K. Characterization of ferrocene-modified electrode using electrochemical surface forces apparatus. *Langmuir* **30**, 7093-7097, doi:10.1021/la5009347 (2014).

98 Kasuya, M. *et al.* Anion Adsorption on Gold Electrodes Studied by Electrochemical Surface Forces Measurement. *J. Phys. Chem. C* **120**, 15986-15992, doi:10.1021/acs.jpcc.5b12683 (2016).

99 Tolansky, S. *Multiple-beam interference microscopy of metals*. (Academic Press Inc. Ltd., Berkeley Square House, London., 1970).

100 Kawai, H. *et al.* New surface forces apparatus using two-beam interferometry. *Rev. Sci. Instrum.* **79**, 043701 (2008).

101 Frantz, P. *et al.* Design of surface forces apparatus for tribology studies combined with nonlinear optical spectroscopy. *Rev. Sci. Instrum.* **68**, 2499-2504 (1997).

102 Frantz, P., Agrait, N. & Salmeron, M. Use of Capacitance to Measure Surface Forces. 1. Measuring Distance of Separation with Enhanced Spatial and Time Resolution. *Langmuir* **12**, 3289-3294, doi:10.1021/la960014b (1996).

103 Parker, J. L. A novel method for measuring the force between two surfaces in a surface force apparatus. *Langmuir* **8**, 551-556, doi:10.1021/la00038a040 (1992).

104 Levins, J. M. & Vanderlick, T. K. Extended Spectral analysis of multiple beam interferometry: a technique to study metallic films in the surface forces apparatus. *Langmuir* **10**, 2389-2394 (1994).

105 Lecadre, F., Kasuya, M., Harano, A., Kanno, Y. & Kurihara, K. Low-Temperature Surface Forces Apparatus to Determine the Interactions between Ice and Silica Surfaces. *Langmuir* **34**, 11311-11315, doi:10.1021/acs.langmuir.8b01902 (2018).

106 Lecadre, F. *et al.* Ice premelting layer of ice-rubber friction studied using resonance shear measurement. *Soft Matter* **16**, 8677-8682, doi:10.1039/d0sm00478b (2020).

107 Crassous, J., Charlaix, E. & Loubet, J.-L. Nanoscale investigation of wetting dynamics with a surface force apparatus. *Phys. Rev. Lett.* **78**, 2425 (1997).

108 Briscoe, W. H. & Horn, R. G. Direct Measurement of Surface Forces Due to Charging of Solids Immersed in a Nonpolar Liquid. *Langmuir* **18**, 3945-3956, doi:10.1021/la015657s (2002).

109 Klein, J. & Kumacheva, E. Simple liquids confined to molecularly thin layers. I. Confinement-induced liquid-to-solid phase transitions. *J. Chem. Phys.* **108**, 6996-7009, doi:10.1063/1.476114 (1998).

110 Berman, A. D., Ducker, W. A. & Israelachvili, J. N. Origin and Characterization of Different Stick−Slip Friction Mechanisms. *Langmuir* **12**, 4559-4563, doi:10.1021/la950896z (1996).

111 Kienle, D. F. & Kuhl, T. L. Density and Phase State of a Confined Nonpolar Fluid. *Phys. Rev. Lett.* **117**, 036101, doi:10.1103/PhysRevLett.117.036101 (2016).

112 Bureau, L. Nonlinear rheology of a nanoconfined simple fluid. *Phys. Rev. Lett.* **104**, 218302 (2010).

113 Horn, R., Evans, D. & Ninham, B. Double-layer and solvation forces measured in a molten salt and its mixtures with water. *J. Phys. Chem.* **92**, 3531-3537 (1988).

114 Bou-Malham, I. & Bureau, L. Nanoconfined ionic liquids: effect of surface charges on flow and molecular layering. *Soft Matter* **6**, 4062-4065 (2010).

115 Ueno, K., Kasuya, M., Watanabe, M., Mizukami, M. & Kurihara, K. Resonance shear measurement of nanoconfined ionic liquids. *Phys. Chem. Chem. Phys.* **12**, 4066-4071 (2010).

116 Perkin, S. *et al.* Self-assembly in the electrical double layer of ionic liquids. *Chem. Commun.* **47**, 6572-6574 (2011).

117 Perkin, S., Albrecht, T. & Klein, J. Layering and shear properties of an ionic liquid, 1-ethyl-3-methylimidazolium ethylsulfate, confined to nano-films between mica surfaces. *Phys. Chem. Chem. Phys.* **12**, 1243-1247 (2010).

118 Cui, S., Cummings, P. & Cochran, H. Molecular simulation of the transition from liquidlike to solidlike behavior in complex fluids confined to nanoscale gaps. *J. Chem. Phys.* **114**, 7189-7195 (2001).

119 Cummings, P. T., Docherty, H., Iacovella, C. R. & Singh, J. K. Phase transitions in nanoconfined fluids: The evidence from simulation and theory. *AIChE J.* **56**, 842-848 (2010).

120 Christenson, H., Gruen, D., Horn, R. & Israelachvili, J. Structuring in liquid alkanes between solid surfaces: Force measurements and mean‐field theory. *J. Chem. Phys.* **87**, 1834-1841 (1987).

121 Demirel, A. L. & Granick, S. Transition from static to kinetic friction in a model lubricated system. *J. Chem. Phys.* **109**, 6889-6897 (1998).

122 Klein, J. Frictional dissipation in stick-slip sliding. *Phys. Rev. Lett.* **98**, 056101 (2007).

123 Smith, A. M., Lovelock, K. R., Gosvami, N. N., Welton, T. & Perkin, S. Quantized friction across ionic liquid thin films. *Phys. Chem. Chem. Phys.* **15**, 15317-15320 (2013).

124 Lhermerout, R. & Perkin, S. A new methodology for a detailed investigation of quantized friction in ionic liquids. *Phys. Chem. Chem. Phys.* **22**, 455-466 (2020).

125 Diestler, D. J., Schoen, M. & Cushman, J. H. On the thermodynamic stability of confined thin films under shear. *Science* **262**, 545-547 (1993).

126 Gee, M. L., McGuiggan, P. M., Israelachvili, J. N. & Homola, A. M. Liquid to solidlike transitions of molecularly thin films under shear. *J. Chem. Phys.* **93**, 1895-1906 (1990).

127 Urbakh, M., Klafter, J., Gourdon, D. & Israelachvili, J. The nonlinear nature of friction. *Nature* **430**, 525-528 (2004).

128 Lei, Y. & Leng, Y. Stick-slip friction and energy dissipation in boundary lubrication. *Phys. Rev. Lett.* **107**, 147801 (2011).

129 Lee, D. W., Banquy, X. & Israelachvili, J. N. Stick-slip friction and wear of articular joints. *Proc. Natl. Acad. Sci.* **110**, E567-E574 (2013).

130 Vanossi, A., Manini, N., Urbakh, M., Zapperi, S. & Tosatti, E. Colloquium: Modeling friction: From nanoscale to mesoscale. *Rev. Mod. Phys.* **85**, 529 (2013).

131 Thompson, P. A. & Robbins, M. O. Origin of stick-slip motion in boundary lubrication. *Science* **250**, 792-794 (1990).

132 Rosenhek-Goldian, I., Kampf, N., Yeredor, A. & Klein, J. On the question of whether lubricants fluidize in stick-slip friction. *Proc. Natl. Acad. Sci.* **112**, 7117-7122, doi:10.1073/pnas.1505609112 (2015).

133 Xu, R.-G. & Leng, Y. Squeezing and stick–slip friction behaviors of lubricants in boundary lubrication. *Proc. Natl. Acad. Sci.* **115**, 6560-6565 (2018).

134 Smith, A. M., Hallett, J. E. & Perkin, S. Solidification and superlubricity with molecular alkane films. *Proc. Natl. Acad. Sci.* **116**, 25418-25423 (2019).

135 Van Alsten, J. & Granick, S. Molecular tribometry of ultrathin liquid films. *Phys. Rev. Lett.* **61**, 2570 (1988).

136 Migler, K., Hervet, H. & Leger, L. Slip transition of a polymer melt under shear stress. *Phys. Rev. Lett.* **70**, 287 (1993).

137 Hod, O., Meyer, E., Zheng, Q. & Urbakh, M. Structural superlubricity and ultralow friction across the length scales. *Nature* **563**, 485-492 (2018).

138 Rogers, R. D. & Seddon, K. R. Ionic liquids--solvents of the future? *Science* **302**, 792-793 (2003).

139 Rakov, D. A. *et al.* Engineering high-energy-density sodium battery anodes for improved cycling with superconcentrated ionic-liquid electrolytes. *Nat. Mater.* **19**, 1096-1101 (2020).

140 MacFarlane, D. R. *et al.* Energy applications of ionic liquids. *Energy & Environmental Science* **7**, 232-250 (2014).

141 Zhou, F., Liang, Y. & Liu, W. Ionic liquid lubricants: designed chemistry for engineering applications. *Chem. Soc. Rev.* **38**, 2590-2599 (2009).

142 Somers, A. E., Howlett, P. C., MacFarlane, D. R. & Forsyth, M. A review of ionic liquid lubricants. *Lubricants* **1**, 3-21 (2013).

143 Ghandi, K. A review of ionic liquids, their limits and applications. *Green Sustain. Chem.* **2014** (2014).

144 Lei, Z., Chen, B., Koo, Y.-M. & MacFarlane, D. R. Introduction: ionic liquids. *Chem. Rev.* **117**, 6633-6635 (2017).

145 Perkin, S. Ionic liquids in confined geometries. *Phys. Chem. Chem. Phys.* **14**, 5052-5062 (2012).

146 Mezger, M. *et al.* Molecular layering of fluorinated ionic liquids at a charged sapphire (0001) surface. *Science* **322**, 424-428 (2008).

147 Gebbie, M. A., Dobbs, H. A., Valtiner, M. & Israelachvili, J. N. Long-range electrostatic screening in ionic liquids. *Proc. Natl. Acad. Sci.* **112**, 7432-7437 (2015).

148 Gebbie, M. A. *et al.* Long range electrostatic forces in ionic liquids. *Chem. Commun.* **53**, 1214-1224 (2017).

149 Jurado, L. A. *et al.* Irreversible structural change of a dry ionic liquid under nanoconfinement. *Phys. Chem. Chem. Phys.* **17**, 13613-13624, doi:10.1039/c4cp05592f (2015).

150 Ye, C., Liu, W., Chen, Y. & Yu, L. Room-temperature ionic liquids: a novel versatile lubricant. *Chem. Commun.* **47**, 2244-2245 (2001).

151 Espinosa-Marzal, R. M., Arcifa, A., Rossi, A. & Spencer, N. D. Microslips to "Avalanches" in Confined, Molecular Layers of Ionic Liquids. *J. Phys. Chem. Lett.* **5**, 179-184, doi:10.1021/jz402451v (2014).

152 Smith, A. M., Parkes, M. A. & Perkin, S. Molecular friction mechanisms across nanofilms of a bilayer-forming ionic liquid. *J. Phys. Chem. Lett.* **5**, 4032-4037 (2014).

153 Han, M. W. & Espinosa-Marzal, R. M. Molecular Mechanisms Underlying Lubrication by Ionic Liquids: Activated Slip and Flow. *Lubricants* **6**, 64, doi:10.3390/lubricants6030064 (2018).

154 Lhermerout, R., Diederichs, C. & Perkin, S. Are ionic liquids good boundary lubricants? A molecular perspective. *Lubricants* **6**, 9 (2018).

155 Perez-Martinez, C. S. & Perkin, S. Interfacial Structure and Boundary Lubrication of a Dicationic Ionic Liquid. *Langmuir* **35**, 15444-15450, doi:10.1021/acs.langmuir.9b01415 (2019).

156 Israelachvili, J. N., McGuiggan, P. M. & Homola, A. M. Dynamic properties of molecularly thin

liquid films. *Science* **240**, 189-191 (1988).

157 Greaves, T. L. & Drummond, C. J. Ionic liquids as amphiphile self-assembly media. *Chem. Soc. Rev.* **37**, 1709-1726 (2008).

158 Hayes, R., Warr, G. G. & Atkin, R. Structure and nanostructure in ionic liquids. *Chem. Rev.* **115**, 6357-6426 (2015).

159 Espinosa-Marzal, R. M., Arcifa, A., Rossi, A. & Spencer, N. D. Ionic Liquids Confined in Hydrophilic Nanocontacts: Structure and Lubricity in the Presence of Water. *J. Phys. Chem. C* **118**, 6491-6503, doi:10.1021/jp5000123 (2014).

160 Raviv, U., Laurat, P. & Klein, J. Fluidity of water confined to subnanometre films. *Nature* **413**, 51-54 (2001).

161 Jagla, E. Boundary lubrication properties of materials with expansive freezing. *Phys. Rev. Lett.* **88**, 245504 (2002).

162 Klein, J. Hydration lubrication. *Friction* **1**, 1-23, doi:10.1007/s40544-013-0001-7 (2013).

163 Rand, R. & Parsegian, V. Hydration forces between phospholipid bilayers. *Biochimica et Biophysica Acta (BBA)-Reviews on Biomembranes* **988**, 351-376 (1989).

164 Ma, L., Gaisinskaya-Kipnis, A., Kampf, N. & Klein, J. Origins of hydration lubrication. *Nat. Commun.* **6**, 6060, doi:10.1038/ncomms7060 (2015).

165 Gaisinskaya-Kipnis, A., Ma, L., Kampf, N. & Klein, J. Frictional Dissipation Pathways Mediated by Hydrated Alkali Metal Ions. *Langmuir* **32**, 4755-4764, doi:10.1021/acs.langmuir.6b00707 (2016).

166 Schlaich, A., Kappler, J. & Netz, R. R. Hydration Friction in Nanoconfinement: From Bulk via Interfacial to Dry Friction. *Nano Lett.* **17**, 5969-5976, doi:10.1021/acs.nanolett.7b02000 (2017).

167 Kang, T. *et al.* Mussel-Inspired Anchoring of Polymer Loops That Provide Superior Surface Lubrication and Antifouling Properties. *ACS Nano* **10**, 930-937, doi:10.1021/acsnano.5b06066 (2016).

168 Morgese, G., Cavalli, E., Müller, M., Zenobi-Wong, M. & Benetti, E. M. Nanoassemblies of tissue-reactive, polyoxazoline graft-copolymers restore the lubrication properties of degraded cartilage. *ACS Nano* **11**, 2794-2804 (2017).

169 Zhu, L. Y., Seror, J., Day, A. J., Kampf, N. & Klein, J. Ultra-low friction between boundary layers of hyaluronan-phosphatidylcholine complexes. *Acta Biomater.* **59**, 283-292, doi:10.1016/j.actbio.2017.06.043 (2017).

170 Veeregowda, D. H. *et al.* Recombinant supercharged polypeptides restore and improve biolubrication. *Adv. Mater.* **25**, 3426-3431 (2013).

171 Yuan, S., Chen, X. & Zhang, C. Reducing Friction by Control of Isoelectric Point: A Potential Method to Design Artificial Cartilage. *Advanced Materials Interfaces* **7**, 2000485 (2020).

172 Xia, Y. *et al.* Biomimetic Bottlebrush Polymer Coatings for Fabrication of Ultralow Fouling Surfaces. *Angew. Chem.* **58**, 1308-1314, doi:10.1002/anie.201808987 (2019).

173 Andresen Eguiluz, R. C. *et al.* Fibronectin mediates enhanced wear protection of lubricin during shear. *Biomacromolecules* **16**, 2884-2894, doi:10.1021/acs.biomac.5b00810 (2015).

174 Seror, J. *et al.* Articular Cartilage Proteoglycans As Boundary Lubricants: Structure and Frictional Interaction of Surface-Attached Hyaluronan and Hyaluronan-Aggrecan Complexes. *Biomacromolecules* **12**, 3432-3443, doi:10.1021/bm2004912 (2011).

175 Seror, J. *et al.* Normal and Shear Interactions between Hyaluronan-Aggrecan Complexes Mimicking Possible Boundary Lubricants in Articular Cartilage in Synovial Joints.

Biomacromolecules **13**, 3823-3832, doi:10.1021/bm301283f (2012).

176 Zheng, Y. *et al.* Bioinspired hyaluronic acid/phosphorylcholine polymer with enhanced lubrication and anti-inflammation. *Biomacromolecules* **20**, 4135-4142 (2019).

177 Shoaib, T., Yuh, C., Wimmer, M. A., Schmid, T. M. & Espinosa-Marzal, R. M. Nanoscale insight into the degradation mechanisms of the cartilage articulating surface preceding OA. *Biomater Sci* **8**, 3944-3955, doi:10.1039/d0bm00496k (2020).

178 Faivre, J. *et al.* Intermolecular interactions between bottlebrush polymers boost the protection of surfaces against frictional wear. *Chem. Mater.* **30**, 4140-4149 (2018).

179 Wang, Z. *et al.* Investigation of the lubrication properties and synergistic interaction of biocompatible liposome-polymer complexes applicable to artificial joints. *Colloids and Surfaces B: Biointerfaces* **178**, 469-478 (2019).

180 Briscoe, W. H. Aqueous boundary lubrication: Molecular mechanisms, design strategy, and terra incognita. *Curr. Opin. Colloid Interface Sci.* **27**, 1-8 (2017).

181 Coles, J. M., Chang, D. P. & Zauscher, S. Molecular mechanisms of aqueous boundary lubrication by mucinous glycoproteins. *Curr. Opin. Colloid Interface Sci.* **15**, 406-416 (2010).

182 Liu, G., Cai, M., Zhou, F. & Liu, W. Charged polymer brushes-grafted hollow silica nanoparticles as a novel promising material for simultaneous joint lubrication and treatment. *J. Phys. Chem. B* **118**, 4920-4931 (2014).

183 Han, T., Zhang, C. & Luo, J. Macroscale superlubricity enabled by hydrated alkali metal ions. *Langmuir* **34**, 11281-11291 (2018).

184 Wang, C.-S., Xie, R., Liu, S. & Giasson, S. Tribological Behavior of Surface-Immobilized Novel Biomimicking Multihierarchical Polymers: The Role of Structure and Surface Attachment. *Langmuir* **35**, 15592-15604, doi:10.1021/acs.langmuir.9b02018 (2019).

185 Lin, W. *et al.* Cartilage-inspired, lipid-based boundary-lubricated hydrogels. *Science* **370**, 335-338 (2020).

186 Lin, W. F., Liu, Z., Kampf, N. & Klein, J. The Role of Hyaluronic Acid in Cartilage Boundary Lubrication. *Cells* **9**, doi:10.3390/cells9071606 (2020).

187 Lin, W. *et al.* Lipid-hyaluronan synergy strongly reduces intrasynovial tissue boundary friction. *Acta Biomater.* **83**, 314-321 (2019).

188 Giasson, S., Lagleize, J. M., Rodriguez-Hernandez, J. & Drummond, C. Boundary lubricant polymer films: effect of cross-linking. *Langmuir* **29**, 12936-12949, doi:10.1021/la402074n (2013).

189 Liao, W. P., Elliott, I. G., Faller, R. & Kuhl, T. L. Normal and shear interactions between high grafting density polymer brushes grown by atom transfer radical polymerization. *Soft Matter* **9**, 5753-5761, doi:10.1039/c3sm50261a (2013).

190 Liu, X. *et al.* Low friction and high load bearing capacity layers formed by cationic-block-non-ionic bottle-brush copolymers in aqueous media. *Soft Matter* **9**, 5361-5371 (2013).

191 Washizu, H., Kinjo, T. & Yoshida, H. Structure of polyelectrolyte brushes studied by coarse grain simulations. *Friction* **2**, 73-81 (2014).

192 Kampf, N., Wu, C., Wang, Y. & Klein, J. A Trimeric Surfactant: Surface Micelles, Hydration-Lubrication, and Formation of a Stable, Charged Hydrophobic Monolayer. *Langmuir* **32**, 11754-11762, doi:10.1021/acs.langmuir.6b02657 (2016).

193 Li, J. *et al.* AFM studies on liquid superlubricity between silica surfaces achieved with surfactant micelles. *Langmuir* **32**, 5593-5599 (2016).

194 Diao, Y. & Espinosa-Marzal, R. M. The role of water in fault lubrication. *Nat. Commun.* **9**, 2309, doi:10.1038/s41467-018-04782-9 (2018).

195 Daniel, D. *et al.* Hydration lubrication of polyzwitterionic brushes leads to nearly friction-and adhesion-free droplet motion. *Commun. Phys.* **2**, 1-7 (2019).

196 Lin, W. & Klein, J. Control of surface forces through hydrated boundary layers. *Curr. Opin. Colloid Interface Sci.* **44**, 94-106, doi:10.1016/j.cocis.2019.10.001 (2019).

197 Tivony, R., Zhang, Y. & Klein, J. Modulating Interfacial Energy Dissipation via Potential-Controlled Ion Trapping. *J. Phys. Chem. C* **125**, 3616-3622 (2021).

198 Jamadagni, S. N., Godawat, R. & Garde, S. Hydrophobicity of proteins and interfaces: Insights from density fluctuations. *Annu. Rev. Chem. Biomol. Eng.* **2**, 147-171 (2011).

199 Fox, J. M., Zhao, M., Fink, M. J., Kang, K. & Whitesides, G. M. The molecular origin of enthalpy/entropy compensation in biomolecular recognition. *Annu. Rev. Biophys.* **47**, 223-250 (2018).

200 Vazdar, M., Pluharova, E., Mason, P. E., Vácha, R. & Jungwirth, P. Ions at hydrophobic aqueous interfaces: Molecular dynamics with effective polarization. *J. Phys. Chem. Lett.* **3**, 2087-2091 (2012).

201 Schwierz, N., Horinek, D. & Netz, R. R. Anionic and cationic Hofmeister effects on hydrophobic and hydrophilic surfaces. *Langmuir* **29**, 2602-2614 (2013).

202 Scheu, R. *et al.* Charge asymmetry at aqueous hydrophobic interfaces and hydration shells. *Angew. Chem.* **126**, 9714-9717 (2014).

203 Gan, W. *et al.* The behavior of hydroxide and hydronium ions at the hexadecane–water interface studied with second harmonic generation and zeta potential measurements. *Soft Matter* **13**, 7962-7968 (2017).

204 Manciu, M., Manciu, F. S. & Ruckenstein, E. On the surface tension and Zeta potential of electrolyte solutions. *Adv. Colloid Interface Sci.* **244**, 90-99 (2017).

205 Beattie, J. K., Djerdjev, A. M. & Warr, G. G. The surface of neat water is basic. *Faraday Discuss.* **141**, 31-39 (2009).

206 Kudin, K. N. & Car, R. Why are water− hydrophobic interfaces charged? *J. Am. Chem. Soc.* **130**, 3915-3919 (2008).

207 Drechsler, A., Petong, N., Zhang, J., Kwok, D. Y. & Grundke, K. Force measurements between Teflon AF and colloidal silica particles in electrolyte solutions. *Colloids Surf. A Physicochem. Eng.* **250**, 357-366 (2004).

208 Donaldson Jr, S. H. *et al.* Asymmetric electrostatic and hydrophobic–hydrophilic interaction forces between mica surfaces and silicone polymer thin films. *ACS Nano* **7**, 10094-10104 (2013).

209 Rosenhek-Goldian, I., Kampf, N. & Klein, J. Trapped Aqueous Films Lubricate Highly Hydrophobic Surfaces. *ACS Nano* **12**, 10075-10083, doi:10.1021/acsnano.8b04735 (2018).

210 Petersen, M. K., Iyengar, S. S., Day, T. J. & Voth, G. A. The hydrated proton at the water liquid/vapor interface. *J. Phys. Chem. B* **108**, 14804-14806 (2004).

211 Petersen, P. B. & Saykally, R. J. Evidence for an enhanced hydronium concentration at the liquid water surface. *J. Phys. Chem. B* **109**, 7976-7980 (2005).

212 Duignan, T. T., Parsons, D. F. & Ninham, B. W. Hydronium and hydroxide at the air–water interface with a continuum solvent model. *Chem. Phys. Lett.* **635**, 1-12 (2015).

213 Mamatkulov, S. I., Allolio, C., Netz, R. R. & Bonthuis, D. J. Orientation‐Induced Adsorption of Hydrated Protons at the Air‐Water Interface. *Angew. Chem.* **56**, 15846-15851 (2017).

214 Uematsu, Y., Bonthuis, D. J. & Netz, R. R. Impurity effects at hydrophobic surfaces. *Curr. Opin. Electrochem.* **13**, 166-173 (2019).

215 Smith, A. M., Lee, A. A. & Perkin, S. The electrostatic screening length in concentrated electrolytes increases with concentration. *J. Phys. Chem. Lett.* **7**, 2157-2163 (2016).

216 Adibnia, V. *et al.* Electrostatic Screening Length in "Soft" Electrolyte Solutions. *ACS Macro Lett.* **8**, 1017-1021, doi:10.1021/acsmacrolett.9b00437 (2019).

217 Adar, R. M., Safran, S. A., Diamant, H. & Andelman, D. Screening length for finite-size ions in concentrated electrolytes. *Phys Rev E* **100**, 042615, doi:10.1103/PhysRevE.100.042615 (2019).

218 Zeman, J., Kondrat, S. & Holm, C. Bulk ionic screening lengths from extremely large-scale molecular dynamics simulations. *Chem. Commun.* **56**, 15635-15638, doi:10.1039/d0cc05023g (2020).

219 Cats, P., Evans, R., Härtel, A. & van Roij, R. Primitive model electrolytes in the near and far field: Decay lengths from DFT and simulations. *J. Chem. Phys.* **154**, 124504 (2021).

220 Ciach, A. & Patsahan, O. Correct scaling of the correlation length from a theory for concentrated electrolytes. *arXiv preprint*, arXiv:2102.00878 (2021).

221 JO'm, B. & Reddy, A. *Modern electrochemistry*. (Plenum, 1972).

222 Espinosa-Marzal, R. M., Drobek, T., Balmer, T. & Heuberger, M. P. Hydrated-ion ordering in electrical double layers. *Phys. Chem. Chem. Phys.* **14**, 6085-6093 (2012).

223 Perez-Martinez, C. S., Smith, A. M. & Perkin, S. Scaling analysis of the screening length in concentrated electrolytes. *Phys. Rev. Lett.* **119**, 026002 (2017).

224 Shrestha, B. R. *et al.* Binding mechanism of a de novo coiled coil complex elucidated from surface forces measurements. *J. Colloid Interface Sci.* **581**, 218-225, doi:10.1016/j.jcis.2020.07.097 (2021).

225 Deepankumar, K. *et al.* Supramolecular beta-Sheet Suckerin-Based Underwater Adhesives. *Adv. Funct. Mater.* **30**, doi:10.1002/adfm.201907534 (2020).

226 Lim, C. *et al.* Nanomechanics of Poly(catecholamine) Coatings in Aqueous Solutions. *Angew. Chem.* **55**, 3342-3346, doi:10.1002/anie.201510319 (2016).

227 Gebbie, M. A. *et al.* Tuning underwater adhesion with cation–π interactions. *Nat. Chem.* **9**, 473-479 (2017).

228 Seo, S. *et al.* Significant Performance Enhancement of Polymer Resins by Bioinspired Dynamic Bonding. *Adv. Mater.* **29**, doi:10.1002/adma.201703026 (2017).

229 Zhao, Q. *et al.* Underwater contact adhesion and microarchitecture in polyelectrolyte complexes actuated by solvent exchange. *Nat. Mater.* **15**, 407-412 (2016).

230 Ahn, B. K., Lee, D. W., Israelachvili, J. N. & Waite, J. H. Surface-initiated self-healing of polymers in aqueous media. *Nat. Mater.* **13**, 867-872 (2014).

231 Lee, D. W., Lim, C., Israelachvili, J. N. & Hwang, D. S. Strong Adhesion and Cohesion of Chitosan in Aqueous Solutions. *Langmuir* **29**, 14222-14229, doi:10.1021/la403124u (2013).

232 Lim, C., Hwang, D. S. & Lee, D. W. Intermolecular interactions of chitosan: Degree of acetylation and molecular weight. *Carbohydr. Polym.* **259**, doi:10.1016/j.carbpol.2021.117782 (2021).

233 Faghihnejad, A. *et al.* Adhesion and Surface Interactions of a Self-Healing Polymer with Multiple Hydrogen-Bonding Groups. *Adv. Funct. Mater.* **24**, 2322-2333, doi:10.1002/adfm.201303013 (2014).

234 Yang, X. J., Teng, F. C., Zeng, H. B. & Liu, Y. Impact of cranberry juice on initial adhesion of the EPS producing bacterium Burkholderia cepacia. *Biofouling* **28**, 417-431,

doi:10.1080/08927014.2012.682576 (2012).

235 Natarajan, A. *et al.* Understanding molecular interactions of asphaltenes in organic solvents using a surface force apparatus. *J. Phys. Chem. C* **115**, 16043-16051 (2011).

236 Szilagyi, I., Trefalt, G., Tiraferri, A., Maroni, P. & Borkovec, M. Polyelectrolyte adsorption, interparticle forces, and colloidal aggregation. *Soft Matter* **10**, 2479-2502 (2014).

237 Harvey, N. M., Yakubov, G. E., Stokes, J. R. & Klein, J. Normal and Shear Forces between Surfaces Bearing Porcine Gastric Mucin, a High-Molecular-Weight Glycoprotein. *Biomacromolecules* **12**, 1041-1050, doi:10.1021/bm101369d (2011).

238 Das, S. *et al.* Synergistic Interactions between Grafted Hyaluronic Acid and Lubricin Provide Enhanced Wear Protection and Lubrication. *Biomacromolecules* **14**, 1669-1677, doi:10.1021/bm400327a (2013).

239 Huang, J. *et al.* Probing the Molecular Interactions and Lubrication Mechanisms of Purified Full-Length Recombinant Human Proteoglycan 4 (rhPRG4) and Hyaluronic Acid (HA). *Biomacromolecules* **20**, 1056-1067, doi:10.1021/acs.biomac.8b01678 (2019).

240 Lee, D. W. *et al.* Effects of molecular weight of grafted hyaluronic acid on wear initiation. *Acta Biomater.* **10**, 1817-1823, doi:10.1016/j.actbio.2014.01.013 (2014).

241 Liu, Z. *et al.* Effects of Hyaluronan Molecular Weight on the Lubrication of Cartilage-Emulating Boundary Layers. *Biomacromolecules* **21**, 4345-4354, doi:10.1021/acs.biomac.0c01151 (2020).

242 Zappone, B., Ruths, M., Greene, G. W., Jay, G. D. & Israelachvili, J. N. Adsorption, Lubrication, and Wear of Lubricin on Model Surfaces: Polymer Brush-Like Behavior of a Glycoprotein. *Biophys. J.* **92**, 1693-1708 (2007).

243 Klein, J. Long-ranged surface forces: The structure and dynamics of polymers at interfaces. *Pure Appl. Chem.* **64**, 1577-1584 (1992).

244 Karim, A. & Kumar, S. *Polymer surfaces, interfaces and thin films*. (World Scientific Publishing Company, 2000).

245 Maeda, N., Chen, N., Tirrell, M. & Israelachvili, J. N. Adhesion and friction mechanisms of polymer-on-polymer surfaces. *Science* **297**, 379-382 (2002).

246 Zhang, J., Xiang, L., Yan, B. & Zeng, H. Nanomechanics of Anion−π Interaction in Aqueous Solution. *J. Am. Chem. Soc.* **142**, 1710-1714, doi:10.1021/jacs.9b11552 (2020).

247 Zeng, H., Hwang, D. S., Israelachvili, J. N. & Waite, J. H. Strong reversible Fe3+-mediated bridging between dopa-containing protein films in water. *Proc. Natl. Acad. Sci.* **107**, 12850-12853 (2010).

248 Maier, G. P., Rapp, M. V., Waite, J. H., Israelachvili, J. N. & Butler, A. Adaptive synergy between catechol and lysine promotes wet adhesion by surface salt displacement. *Science* **349**, 628-632 (2015).

249 Lu, Q. Y. *et al.* Nanomechanics of Cation Interactions in Aqueous Solution. *Angew. Chem.* **52**, 3944-3948, doi:10.1002/anie.201210365 (2013).

250 Banquy, X. *et al.* Interaction Forces between Pegylated Star-Shaped Polymers at Mica Surfaces. *ACS Appl. Mater. Interfaces* **9**, 28027-28033, doi:10.1021/acsami.7b06922 (2017).

251 Lin, W., Kampf, N., Goldberg, R., Driver, M. J. & Klein, J. Poly-phosphocholinated liposomes form stable superlubrication vectors. *Langmuir* **35**, 6048-6054 (2019).

252 Xiang, L. *et al.* Probing molecular interactions of PEGylated chitosan in aqueous solutions using a surface force apparatus. *Phys. Chem. Chem. Phys.* **21**, 20571-20581 (2019).

253 Morgese, G. *et al.* Next‐generation polymer shells for inorganic nanoparticles are highly

compact, ultra‐dense, and long‐lasting cyclic brushes. *Angew. Chem.* **56**, 4507-4511 (2017).

254 Klein, J. Shear, friction, and lubrication forces between polymer-bearing surfaces. *Annu. Rev. Mater. Sci.* **26**, 581-612 (1996).

255 Ruhe, J., Novotny, V., Clarke, T. & Street, G. Ultrathin perfluoropolyether films—influence of anchoring and mobility of polymers on the tribological properties. *J. Tribol.* **118**, 663 (1996).

256 Espinosa-Marzal, R. M., Bielecki, R. M. & Spencer, N. D. Understanding the role of viscous solvent confinement in the tribological behavior of polymer brushes: a bioinspired approach. *Soft Matter* **9**, 10572-10585, doi:10.1039/c3sm51415c (2013).

257 Tairy, O., Kampf, N., Driver, M. J., Armes, S. P. & Klein, J. Dense, Highly Hydrated Polymer Brushes via Modified Atom-Transfer-Radical-Polymerization: Structure, Surface Interactions, and Frictional Dissipation. *Macromolecules* **48**, 140-151, doi:10.1021/ma5019439 (2014).

258 Han, M. W. & Espinosa-Marzal, R. M. Strong Stretching of Poly(ethylene glycol) Brushes Mediated by Ionic Liquid Solvation. *J. Phys. Chem. Lett.* **8**, 3954-3960, doi:10.1021/acs.jpclett.7b01451 (2017).

259 Han, L. *et al.* Tuning protein adsorption on charged polyelectrolyte brushes via salinity adjustment. *Colloids Surf. A Physicochem. Eng.* **539**, 37-45 (2018).

260 Shin, E. *et al.* Mussel-Inspired Copolyether Loop with Superior Antifouling Behavior. *Macromolecules* **53**, 3551-3562, doi:10.1021/acs.macromol.0c00481 (2020).

261 Li, L., Yan, B., Zhang, L., Tian, Y. & Zeng, H. Mussel-inspired antifouling coatings bearing polymer loops. *Chem. Commun.* **51**, 15780-15783 (2015).

262 Milner, S. T. Polymer brushes. *Science* **251**, 905-914 (1991).

263 Raviv, U. *et al.* Lubrication by charged polymers. *Nature* **425**, 163-165 (2003).

264 Chen, M., Briscoe, W. H., Armes, S. P. & Klein, J. Lubrication at physiological pressures by polyzwitterionic brushes. *Science* **323**, 1698-1701 (2009).

265 Yu, J. *et al.* Multivalent counterions diminish the lubricity of polyelectrolyte brushes. *Science* **360**, 1434-1438 (2018).

266 Jay, G. D. & Waller, K. A. The biology of Lubricin: Near frictionless joint motion. *Matrix Biol.* **39**, 17-24 (2014).

267 Banquy, X., Burdyńska, J., Lee, D. W., Matyjaszewski, K. & Israelachvili, J. Bioinspired Bottle-Brush Polymer Exhibits Low Friction and Amontons-like Behavior. *J. Am. Chem. Soc.* **136**, 6199-6202, doi:10.1021/ja501770y (2014).

268 Chen, S., Zheng, J., Li, L. & Jiang, S. Strong Resistance of Phosphorylcholine Self-Assembled Monolayers to Protein Adsorption: Insights into Nonfouling Properties of Zwitterionic Materials. *J. Am. Chem. Soc.* **127**, 14473-14478, doi:10.1021/ja054169u (2005).

269 Heggestad, J. T., Fontes, C. M., Joh, D. Y., Hucknall, A. M. & Chilkoti, A. In Pursuit of Zero 2.0: Recent Developments in Nonfouling Polymer Brushes for Immunoassays. *Adv. Mater.* **32**, 1903285 (2020).

270 Serrano, Â. *et al.* Nonfouling Response of Hydrophilic Uncharged Polymers. *Adv. Funct. Mater.* **23**, 5706-5718 (2013).

271 Chen, M., Briscoe, W. H., Armes, S. P., Cohen, H. & Klein, J. Polyzwitterionic brushes: Extreme lubrication by design. *Eur. Polym. J.* **47**, 511-523 (2011).

272 Luckham, P. F. & Klein, J. Forces between mica surfaces bearing adsorbed homopolymers in good solvents. The effect of bridging and dangling tails. *J. Chem. Soc., Faraday Trans.* **86**, 1363-1368, doi:10.1039/FT9908601363 (1990).

273 De Gennes, P. Polymers at an interface; a simplified view. *Adv. Colloid Interface Sci.* **27**, 189-209 (1987).

274 Taunton, H. J., Toprakcioglu, C., Fetters, L. J. & Klein, J. Forces between surfaces bearing terminally anchored polymer chains in good solvents. *Nature* **332**, 712-714 (1988).

275 Iuster, N., Tairy, O., Driver, M. J., Armes, S. P. & Klein, J. Cross-Linking Highly Lubricious Phosphocholinated Polymer Brushes: Effect on Surface Interactions and Frictional Behavior. *Macromolecules* **50**, 7361-7371, doi:10.1021/acs.macromol.7b01423 (2017).

276 Adibnia, V., Olszewski, M., De Crescenzo, G., Matyjaszewski, K. & Banquy, X. Superlubricity of Zwitterionic Bottlebrush Polymers in the Presence of Multivalent Ions. *J. Am. Chem. Soc.* **142**, 14843-14847, doi:10.1021/jacs.0c07215 (2020).

277 Whitesides, G. M. & Grzybowski, B. Self-Assembly at All Scales. *Science* **295**, 2418-2421, doi:10.1126/science.1070821 (2002).

278 Mai, Y. & Eisenberg, A. Self-assembly of block copolymers. *Chem. Soc. Rev.* **41**, 5969-5985, doi:10.1039/C2CS35115C (2012).

279 Böker, A., He, J., Emrick, T. & Russell, T. P. Self-assembly of nanoparticles at interfaces. *Soft Matter* **3**, 1231-1248, doi:10.1039/B706609K (2007).

280 McGorty, R., Fung, J., Kaz, D. & Manoharan, V. N. Colloidal self-assembly at an interface. *Mater. Today* **13**, 34-42 (2010).

281 Esumi, K., Nagahama, T. & Meguro, K. Characterization of cationic surfactant adsorbed layer on silica. *Colloids Surf.* **57**, 149-160 (1991).

282 Lokar, W. J. & Ducker, W. A. Forces between Glass Surfaces in Mixed Cationic−Zwitterionic Surfactant Systems. *Langmuir* **20**, 4553-4558, doi:10.1021/la036459z (2004).

283 Silbert, G., Kampf, N. & Klein, J. Normal and Shear Forces between Charged Solid Surfaces Immersed in Cationic Surfactant Solution: The Role of the Alkyl Chain Length. *Langmuir* **30**, 5097-5104, doi:10.1021/la501315v (2014).

284 Lin, W., Kampf, N. & Klein, J. Designer Nanoparticles as Robust Superlubrication Vectors. *ACS Nano* **14**, 7008–7017 (2020).

285 Drummond, C., Israelachvili, J. & Richetti, P. Friction between two weakly adhering boundary lubricated surfaces in water. *Phys. Rev. E* **67**, 066110, doi:10.1103/PhysRevE.67.066110 (2003).

286 CHRISTENSON, H. K. & CLAESSON, P. M. Cavitation and the Interaction Between Macroscopic Hydrophobic Surfaces. *Science* **239**, 390-392, doi:10.1126/science.239.4838.390 (1988).

287 Wood, J. & Sharma, R. How Long Is the Long-Range Hydrophobic Attraction? *Langmuir* **11**, 4797-4802, doi:10.1021/la00012a035 (1995).

288 Perkin, S., Kampf, N. & Klein, J. Stability of Self-Assembled Hydrophobic Surfactant Layers in Water. *J. Phys. Chem. B* **109**, 3832-3837, doi:10.1021/jp047746u (2005).

289 Silbert, G. *et al.* Long-Ranged Attraction between Disordered Heterogeneous Surfaces. *Phys. Rev. Lett.* **109**, doi:10.1103/PhysRevLett.109.168305 (2012).

290 Lin, Q., Meyer, E. E., Tadmor, M., Israelachvili, J. N. & Kuhl, T. L. Measurement of the Long- and Short-Range Hydrophobic Attraction between Surfactant-Coated Surfaces. *Langmuir* **21**, 251-255, doi:10.1021/la048317q (2005).

291 Meyer, E. E., Lin, Q., Hassenkam, T., Oroudjev, E. & Israelachvili, J. N. Origin of the long-range attraction between surfactant-coated surfaces. *Proc. Natl. Acad. Sci.* **102**, 6839-6842, doi:10.1073/pnas.0502110102 (2005).

292 Meyer, E. E., Lin, Q. & Israelachvili, J. N. Effects of Dissolved Gas on the Hydrophobic Attraction

between Surfactant-Coated Surfaces. *Langmuir* **21**, 256-259, doi:10.1021/la048318i (2005).

293 Zhang, J., Yoon, R.-H., Mao, M. & Ducker, W. A. Effects of Degassing and Ionic Strength on AFM Force Measurements in Octadecyltrimethylammonium Chloride Solutions. *Langmuir* **21**, 5831-5841, doi:10.1021/la047398n (2005).

294 Meyer, E. E., Rosenberg, K. J. & Israelachvili, J. Recent progress in understanding hydrophobic interactions. *Proc. Natl. Acad. Sci.* **103**, 15739-15746, doi:10.1073/pnas.0606422103 (2006).

295 Perkin, S., Kampf, N. & Klein, J. Long-Range Attraction between Charge-Mosaic Surfaces across Water. *Phys. Rev. Lett.* **96**, 038301, doi:10.1103/PhysRevLett.96.038301 (2006).

296 Klein, J. Origins of the long-ranged attraction between surfaces that were rendered hydrophobic by surfactant layers. *Adv. Colloid Interface Sci.* **270**, 261-262, doi:10.1016/j.cis.2019.06.009 (2019).

297 Ben-Yaakov, D., Andelman, D. & Diamant, H. Interaction between heterogeneously charged surfaces: Surface patches and charge modulation. *Phys. Rev. E* **87**, 022402, doi:10.1103/PhysRevE.87.022402 (2013).

298 Bakhshandeh, A., dos Santos, A. P., Diehl, A. & Levin, Y. Interaction between random heterogeneously charged surfaces in an electrolyte solution. *The Journal of chemical physics* **142**, 194707 (2015).

299 Kékicheff, P. The long-range attraction between hydrophobic macroscopic surfaces. *Adv. Colloid Interface Sci.* **270**, 191-215 (2019).

300 Nagle, J. F. *et al.* X-ray structure determination of fully hydrated L alpha phase dipalmitoylphosphatidylcholine bilayers. *Biophys. J.* **70**, 1419-1431 (1996).

301 Ishihara, K. *et al.* Why do phospholipid polymers reduce protein adsorption? *Journal of Biomedical Materials Research: An Official Journal of The Society for Biomaterials, The Japanese Society for Biomaterials, and the Australian Society for Biomaterials* **39**, 323-330 (1998).

302 Yaseen, M., Lu, J., Webster, J. & Penfold, J. The structure of zwitterionic phosphocholine surfactant monolayers. *Langmuir* **22**, 5825-5832 (2006).

303 Foglia, F., Lawrence, M. J., Lorenz, C. D. & McLain, S. E. On the hydration of the phosphocholine headgroup in aqueous solution. *The Journal of chemical physics* **133**, 10B608 (2010).

304 Goldberg, R. *et al.* Boundary lubricants with exceptionally low friction coefficients based on 2D close-packed phosphatidylcholine liposomes. *Adv. Mater.* **23**, 3517-3521, doi:10.1002/adma.201101053 (2011).

305 Goldberg, R., Schroeder, A., Barenholz, Y. & Klein, J. Interactions between Adsorbed Hydrogenated Soy Phosphatidylcholine (HSPC) Vesicles at Physiologically High Pressures and Salt Concentrations. *Biophys. J.* **100**, 2403-2411, doi:10.1016/j.bpj.2011.03.061 (2011).

306 Sorkin, R., Kampf, N., Zhu, L. & Klein, J. Hydration lubrication and shear-induced self-healing of lipid bilayer boundary lubricants in phosphatidylcholine dispersions. *Soft Matter* **12**, 2773-2784, doi:10.1039/C5SM02475G (2016).

307 Harris, J. M., Martin, N. E. & Modi, M. Pegylation. *Clin. Pharmacokinet.* **40**, 539-551, doi:10.2165/00003088-200140070-00005 (2001).

308 Harris, J. M. & Chess, R. B. Effect of pegylation on pharmaceuticals. *Nat. Rev. Drug Discovery* **2**, 214-221, doi:10.1038/nrd1033 (2003).

309 Lee, S.-Y. & Tong, L. Lipid-Containing Lubricants for Dry Eye: A Systematic Review. *Optom. Vis. Sci.* **89**, 1654-1661, doi:10.1097/OPX.0b013e31826f32e0 (2012).

310 Ji, X. & Zhang, H. Current Strategies for the Treatment of Early Stage Osteoarthritis. *Frontiers in Mechanical Engineering* **5**, doi:10.3389/fmech.2019.00057 (2019).

311 Sarma, A., Powell, G. & LaBerge, M. Phospholipid composition of articular cartilage boundary lubricant. *J. Orthop. Res.* **19**, 671-676 (2001).

312 Kosinska, M. K. *et al.* A lipidomic study of phospholipid classes and species in human synovial fluid. *Arthritis. Rheum.* **65**, 2323-2333 (2013).

313 Seror, J., Zhu, L., Goldberg, R., Day, A. J. & Klein, J. Supramolecular synergy in the boundary lubrication of synovial joints. *Nat. Commun.* **6**, 1-7 (2015).

314 Cao, Y., Kampf, N. & Klein, J. Boundary Lubrication, Hemifusion, and Self-Healing of Binary Saturated and Monounsaturated Phosphatidylcholine Mixtures⧫. *Langmuir* **35**, 15459-15468 (2019).

315 Cao, Y., Kampf, N., Kosinska, M. K., Steinmeyer, J. & Klein, J. Interactions Between Bilayers of Phospholipids Extracted from Human Osteoarthritic Synovial Fluid. *Biotribology* **25**, 100157 (2021).

316 Lin, W. & Klein, J. Recent progress in cartilage lubrication. *Adv. Mater.* **33**, 2005513 (2021).

317 Cao, Y., Kampf, N. & Klein, J. *Submitted*.

318 Schrader, A. M., Cheng, C. Y., Israelachvili, J. N. & Han, S. Communication: Contrasting effects of glycerol and DMSO on lipid membrane surface hydration dynamics and forces. *J. Chem. Phys.* **145**, 041101, doi:10.1063/1.4959904 (2016).

319 Schrader, A. M. *et al.* Correlating steric hydration forces with water dynamics through surface force and diffusion NMR measurements in a lipid–DMSO–H2O system. *Proc. Natl. Acad. Sci.* **112**, 10708-10713 (2015).

320 Lee, D. W. *et al.* Real-time intermembrane force measurements and imaging of lipid domain morphology during hemifusion. *Nat. Commun.* **6**, 7238, doi:10.1038/ncomms8238 (2015).

321 Bartenstein, J. E., Liu, X., Lange, K., Claesson, P. M. & Briscoe, W. H. Polymersomes at the solid-liquid interface: Dynamic morphological transformation and lubrication. *J. Colloid Interface Sci.* **512**, 260-271 (2018).

322 Lin, W. F., Nietzel, S., Klapper, M., Mullen, K. & Klein, J. Normal and shear forces between surfaces bearing phosphocholinated polystyrene nanoparticles. *Polym. Adv. Technol.* **28**, 600-605, doi:10.1002/pat.3859 (2017).

323 Adibnia, V. *et al.* Phytoglycogen Nanoparticles: Nature-Derived Superlubricants. *ACS Nano* **15**, doi.org/10.1021/acsnano.1021c01755 (2021).

324 Jahn, S., Seror, J. & Klein, J. Lubrication of articular cartilage. *Annu. Rev. Biomed. Eng.* **18**, 235-258 (2016).

325 Sun, Z. *et al.* Boundary mode lubrication of articular cartilage with a biomimetic diblock copolymer. *Proc. Natl. Acad. Sci.* **116**, 12437-12441 (2019).

326 Cai, M., Yu, Q., Liu, W. & Zhou, F. Ionic liquid lubricants: when chemistry meets tribology. *Chem. Soc. Rev.* **49**, 7753-7818 (2020).

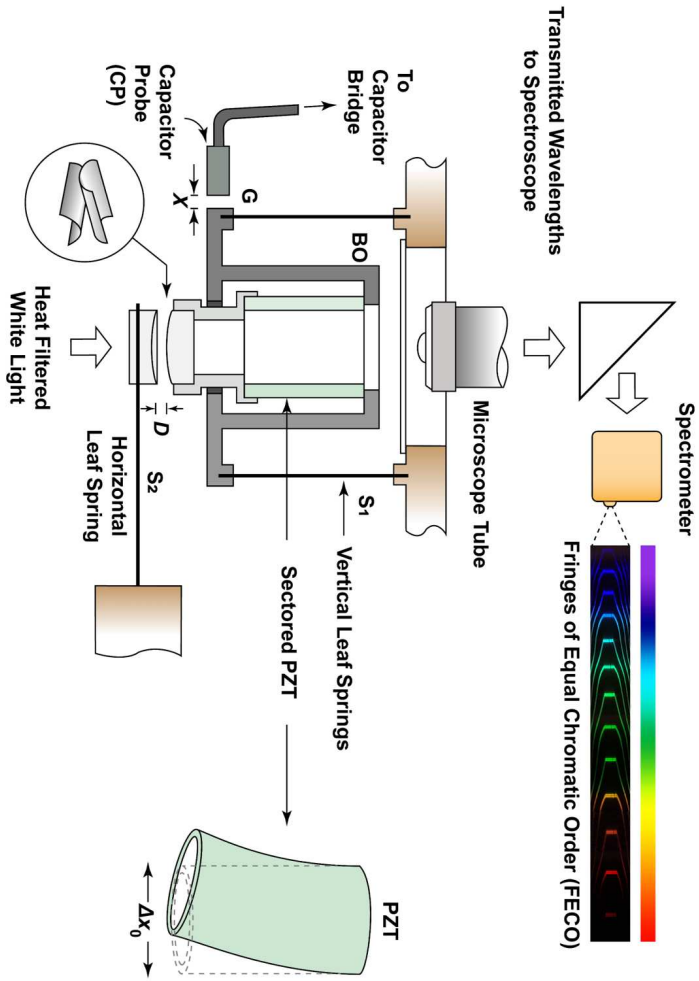

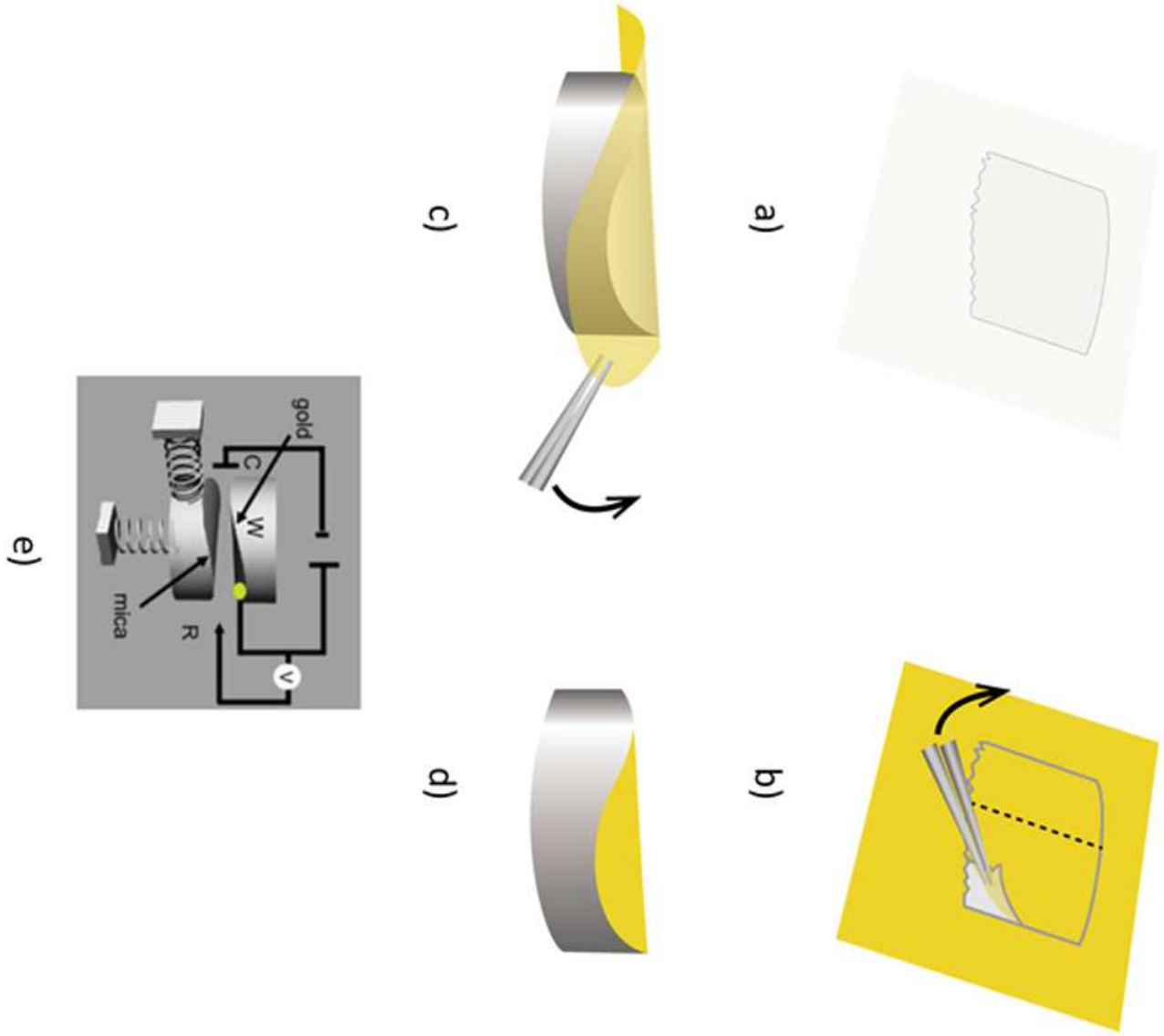

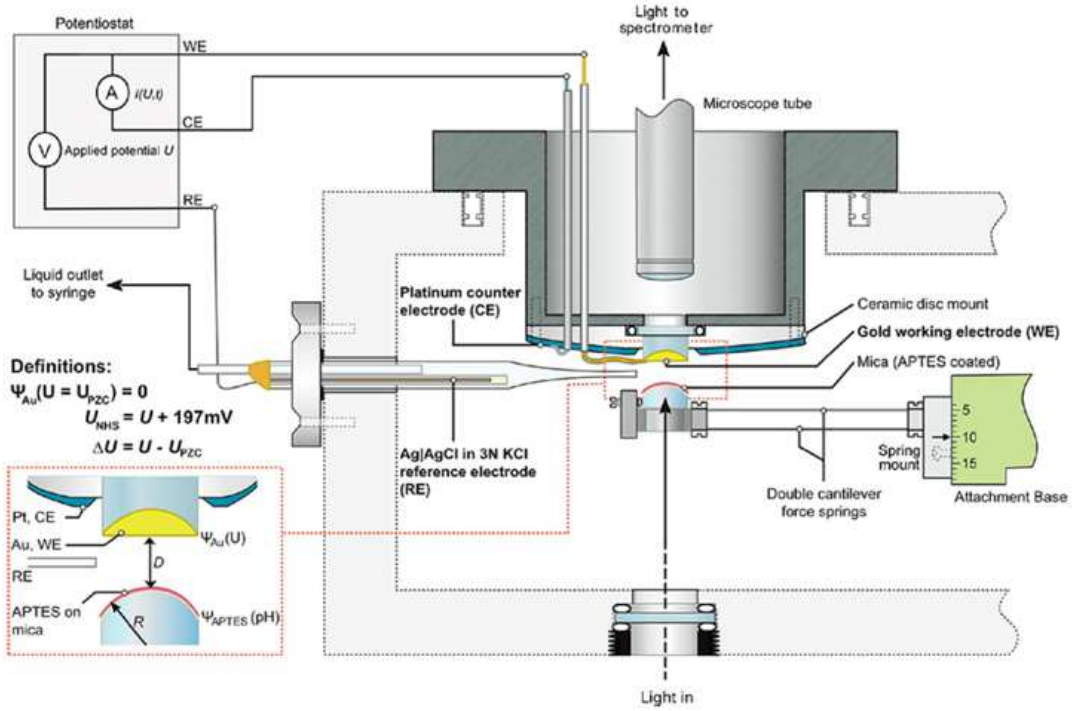

a)

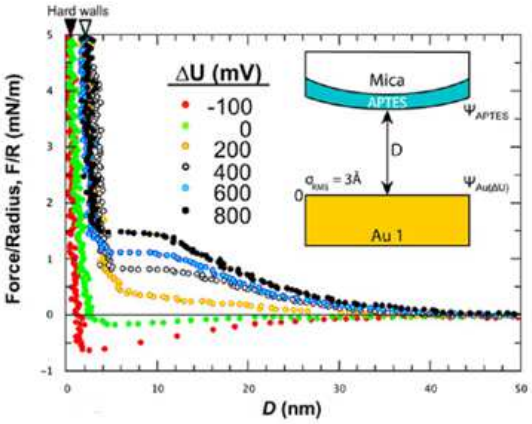

b)

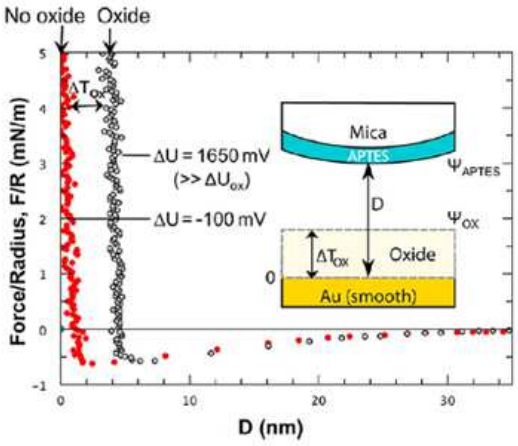

c)

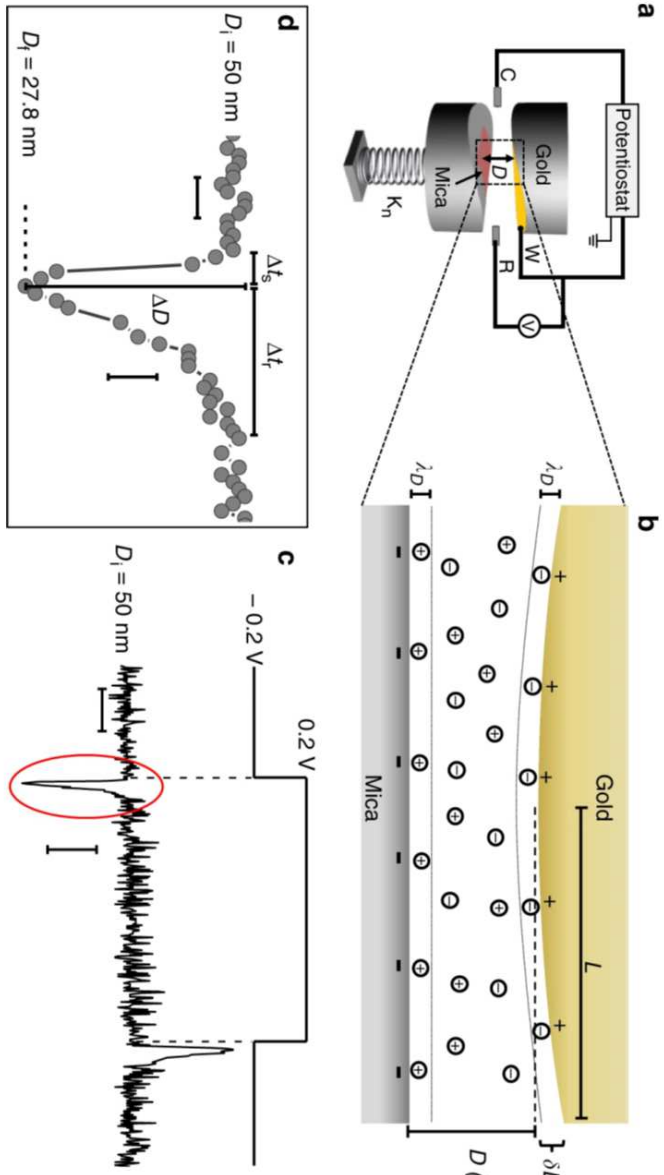

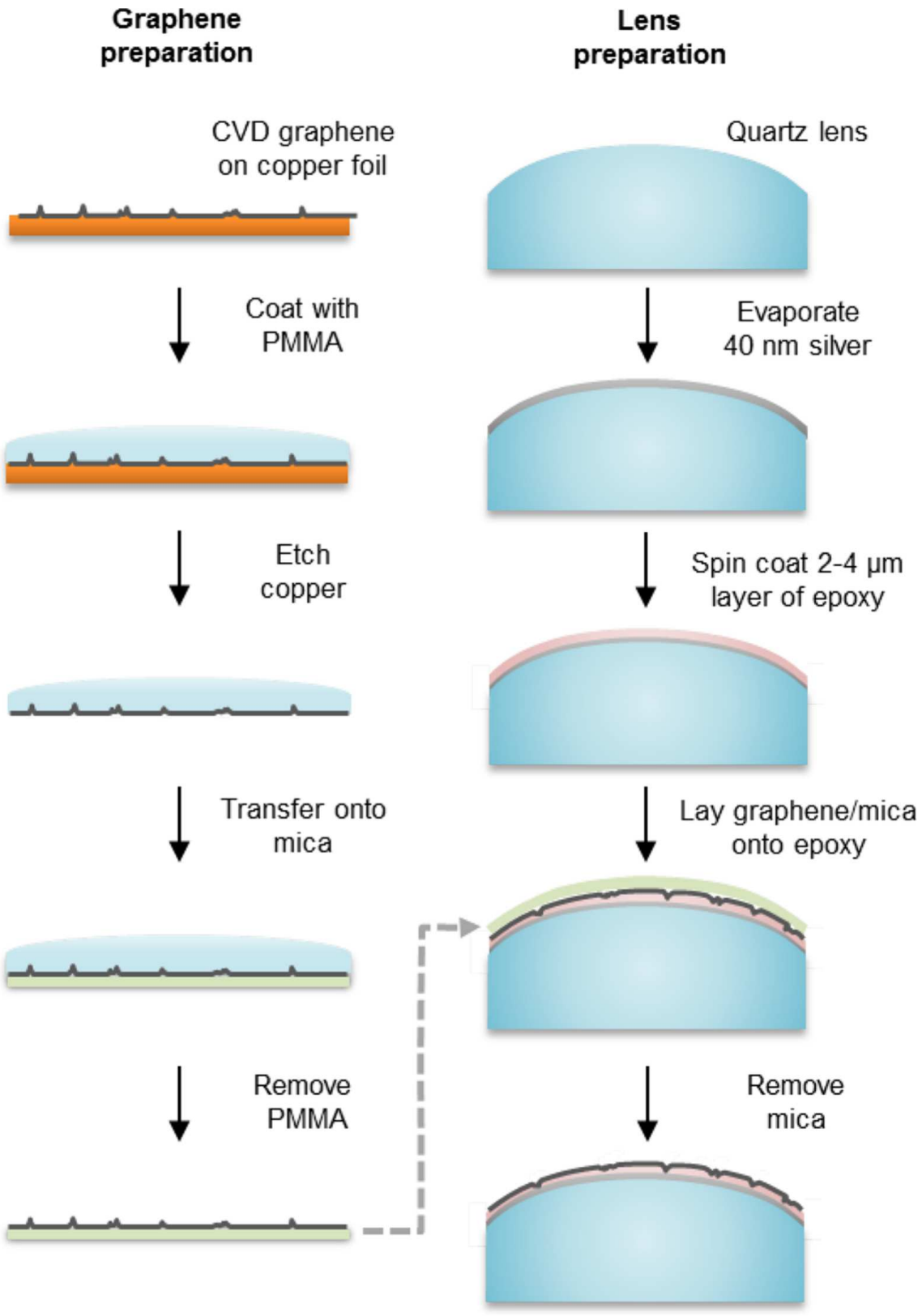

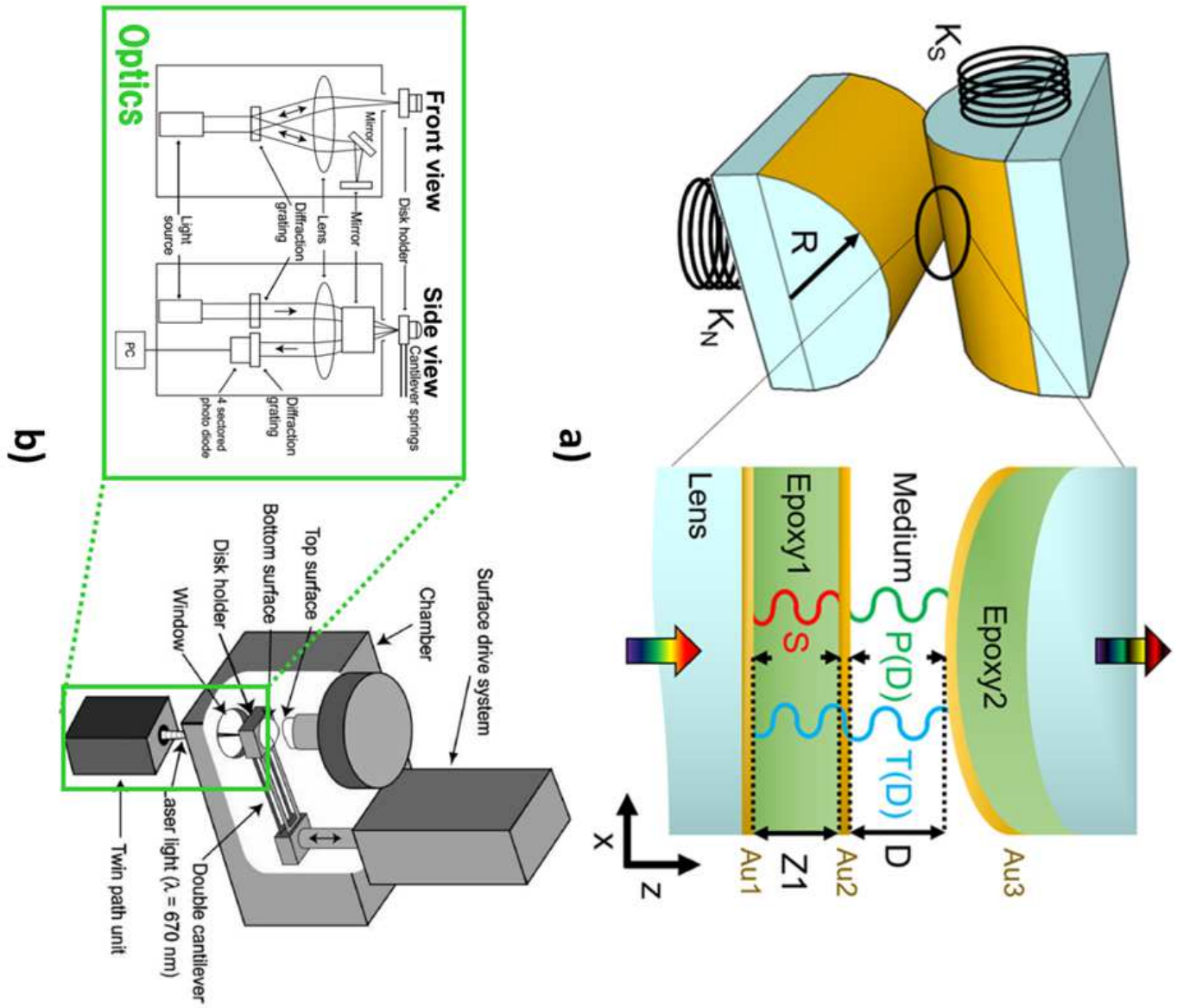

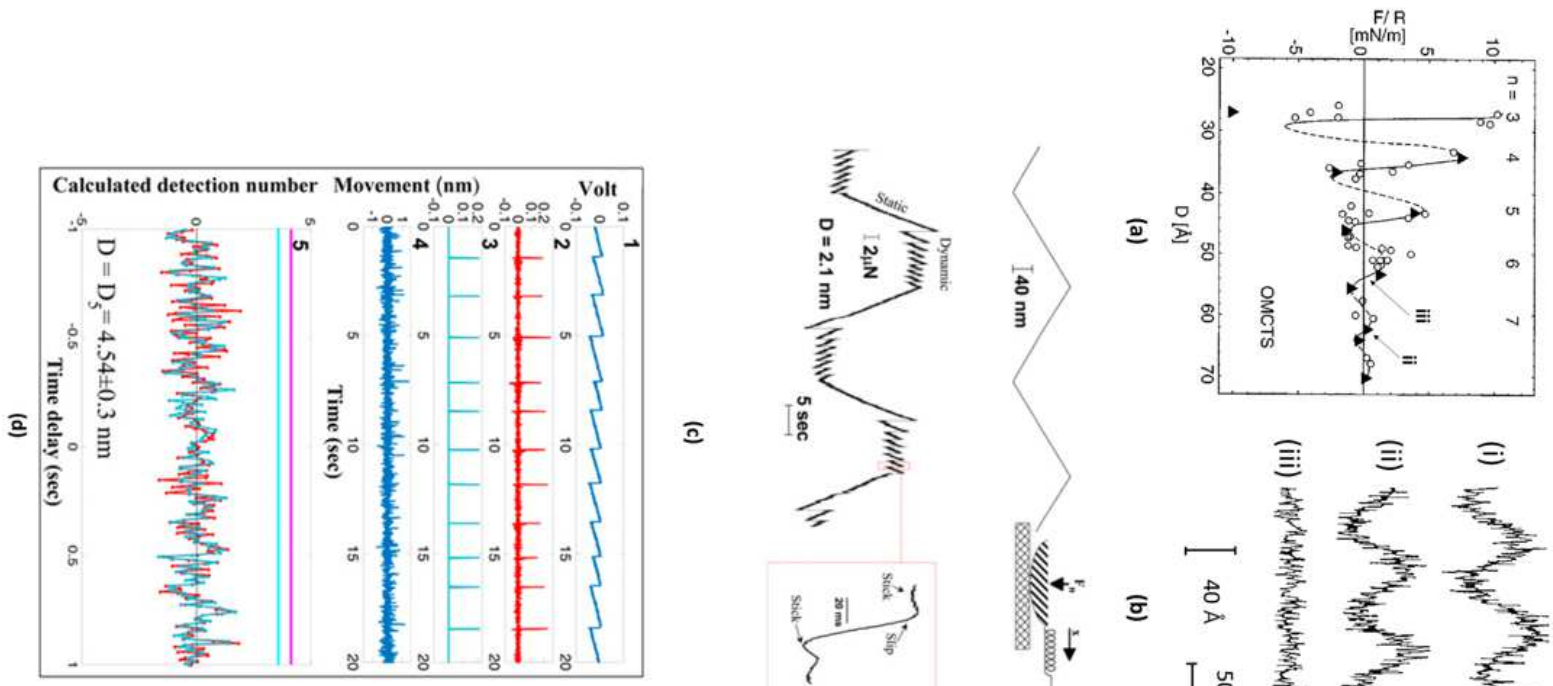

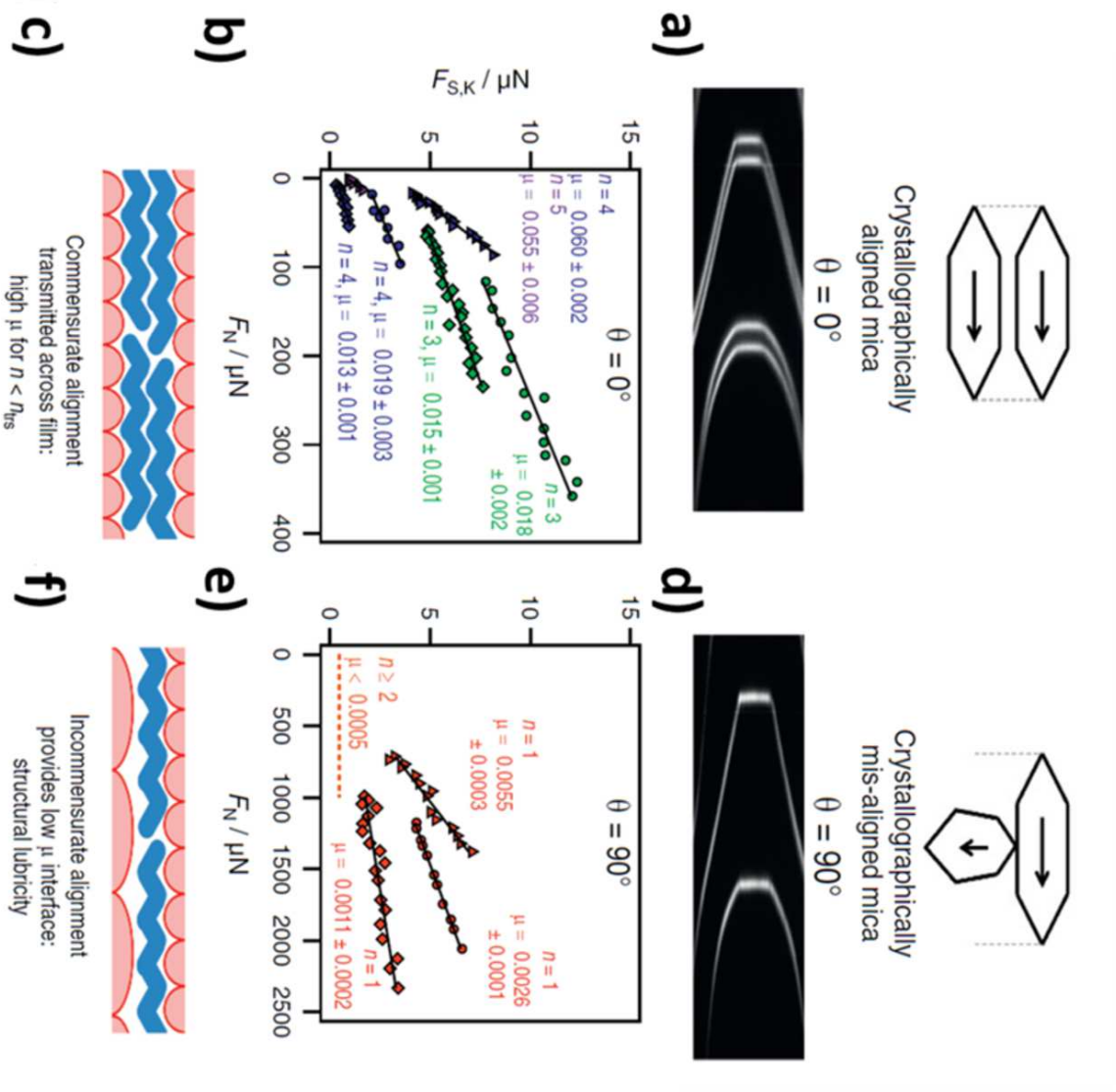

AIP Publishing

Applied Physics Reviews ACCEPTED MANUSCRIPT

PLEASE CITE THIS ARTICLE AS DOI: 10.1063/5.0059893

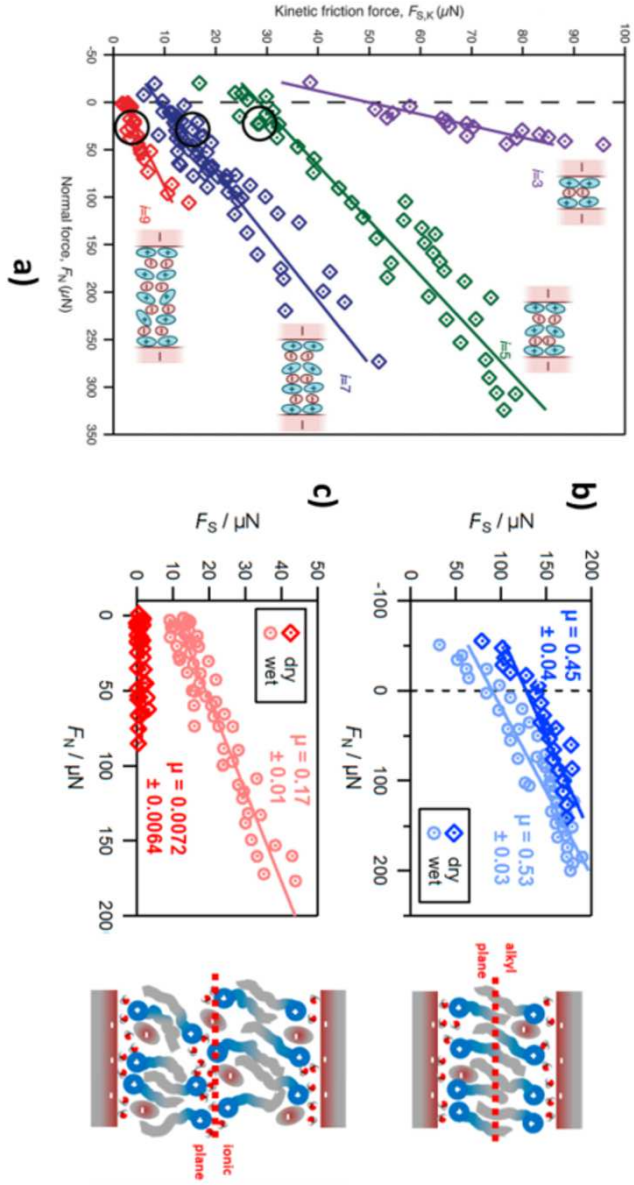

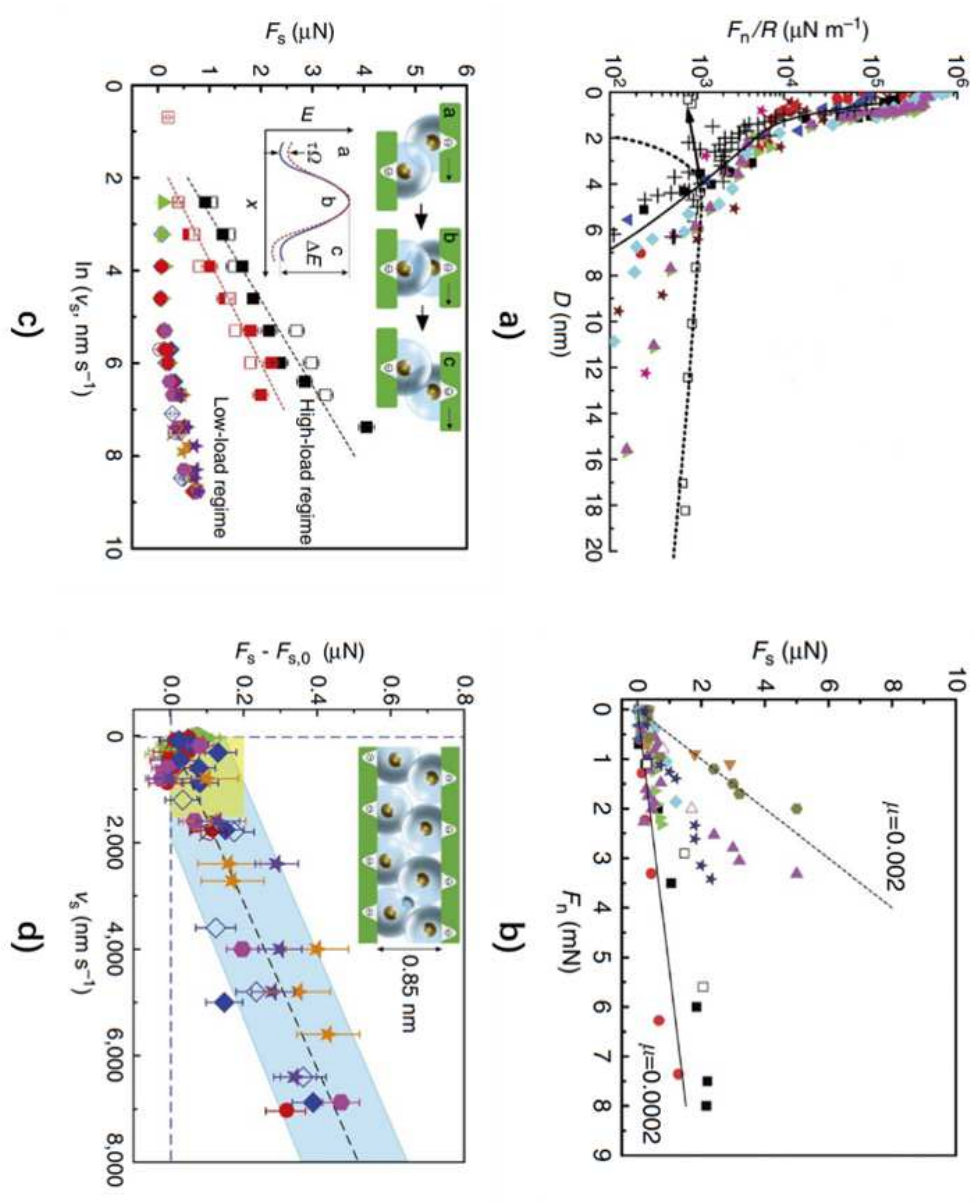

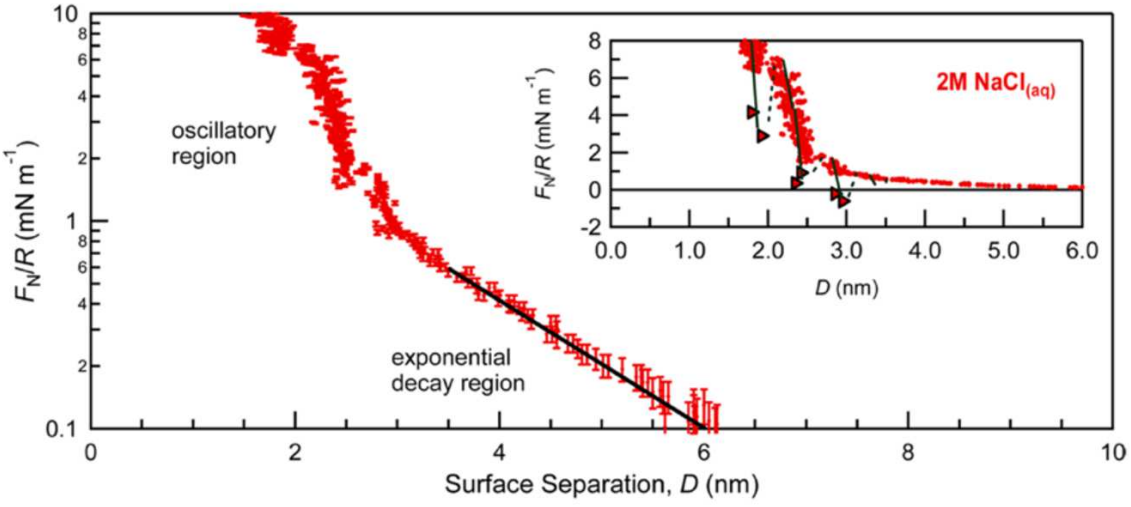

a)

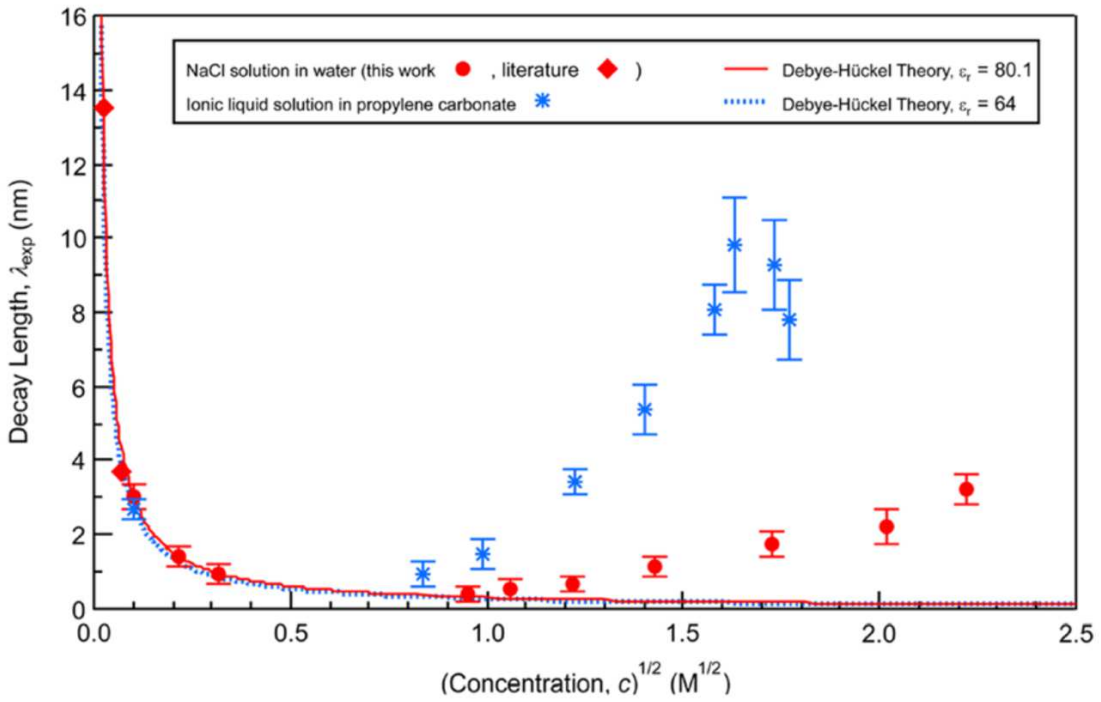

b)